Article

Glycerol mediates crosstalk between metabolism and trafficking through the golgin Imh1

Wan-Yun Chiu[1,2], Yi-Hsun Wang[1,2], Ming-Chieh Lin ®[1,2,3], Chun-Chi Lai[1,2], Chia-Jung Yu ®[4,5] ✉ & Fang-Jen S. Lee ®[1,2,3] ✉

The golgins are long coiled-coil proteins involved in vesicular transport to the Golgi, a process that contributes to Golgi function and integrity. Previous studies have elucidated that their self-interaction and their interaction with small guanosine triphosphatase Arl1 are critical for their Golgi localization but other mechanisms regulating their localization are not identified. Here we report that glycerol promotes Golgi localization of Imh1, a prototypic yeast golgin. We found that various cellular conditions leading to reduced glycerol level release Imh1 from the Golgi and this release is reversed by restoring the intracellular glycerol level. Elucidating how glycerol regulates Imh1 localization, our results suggest that glycerol acts directly on Imh1 to fine-tune its conformation. Furthermore, we show that glycerol also promotes Golgi localization of a mammalian golgin. Thus, our findings reveal a previously unappreciated connection between intracellular metabolism and transport.

The Golgi apparatus acts as a hub in protein traffic within eukaryotic cells, processing and sorting cargos in both the anterograde and the retrograde directions along the secretory pathways[1]. The golgins, which localize to the Golgi, are involved in vesicle transport, cargo selection, Golgi integrity and cytoskeleton organization[2,3]. Members of this protein family share similar structural features, having a long coiled-coil amino terminal region that projects into the cytosolic side of the Golgi membrane and a carboxy terminal region that mediates membrane binding[2,3]. Different golgins are localized to different regions of the Golgi and thereby contribute to the specificity of vesicle trafficking[4]. GRIP (golgin 97, RanBP2α, Imh1p and p230/golgin 245) domain-containing golgins, including mammalian golgin 97, golgin 245/p230, GCC88 and GCC185 and yeast Imh1, are peripheral membrane proteins. Their membrane association is governed by self-interaction, interaction with the small guanosine triphosphatase (GTPase) Arl1 through the GRIP domain and binding to membrane lipids[5–7]. Other

mechanisms that may regulate their targeting to the Golgi remain to be defined.

In yeast, the small GTPase Arl1 is activated by an Arf-GEF known as Syt1, which then recruits Imh1 to the Golgi membrane. Activated Arl1 also participates in a ternary Arl1–Drs2–Gea2 complex that generates a suitable membrane environment for Imh1 Golgi membrane localization[8–11]. Upon the hydrolysis of GTP bound to activated Arl1, which is catalyzed by the GTPase-activating protein (GAP) activity of Gcs1, both Arl1 and Imh1 are released to the cytosol[12]. Imh1 can prolong Arl1 activation at the Golgi by sterically inhibiting the access of Gcs1 toward Arl1 (ref. 12), thereby also promoting its own localization at the Golgi.

We previously found that Imh1 localization can be affected by the unfolded protein response. Endoplasmic reticulum (ER) stress affects retrograde transport to the Golgi mediated by the Golgi-associated retrograde protein (GARP) complex, a process that is dependent on Imh1

[1]Institute of Molecular Medicine, College of Medicine, National Taiwan University, Taipei, Taiwan. [2]Center of Precision Medicine, College of Medicine, National Taiwan University, Taipei, Taiwan. [3]Department of Medical Research, National Taiwan University Hospital, Taipei, Taiwan. [4]Department of Cell and Molecular Biology, College of Medicine, Chang Gung University, Taoyuan, Taiwan. [5]Department of Thoracic Medicine, Chang Gung Memorial Hospital, Taoyuan, Taiwan. ✉e-mail: yucj1124@mail.cgu.edu.tw; fangjen@ntu.edu.tw
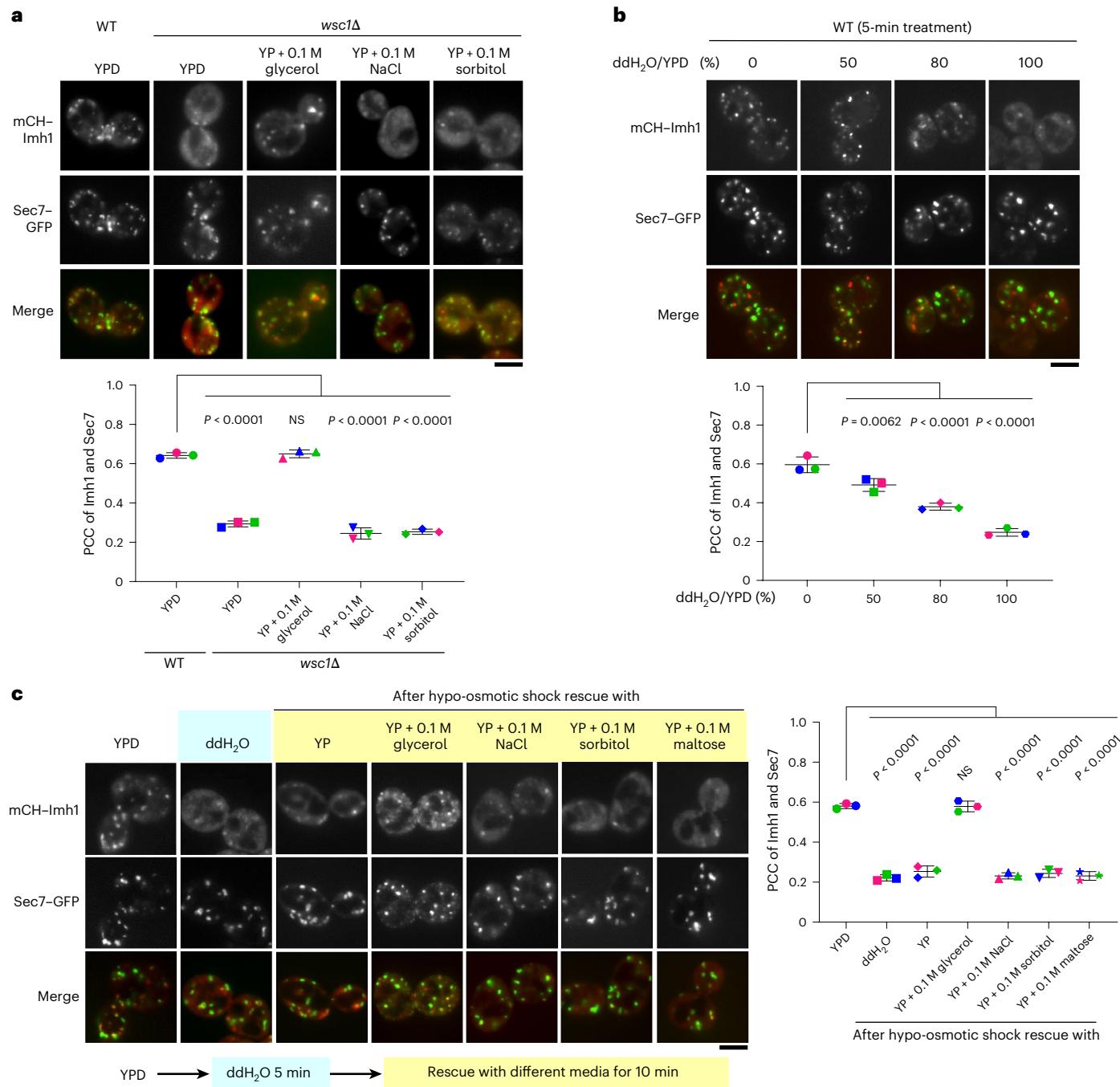
Fig. 1 | Glycerol addition reverses defective Imh1 localization induced by hypo-osmotic shock. a, Glycerol rescues Imh1 mislocalization in *wsc1*Δ cells. mCH–Imh1 was expressed in WT and *wsc1*Δ cells. Cells were grown to midlog phase in YPD medium, the medium was removed and the cells were suspended in YP medium with 0.1 M glycerol, NaCl or sorbitol. **b**, mCH–Imh1 is mislocalized from the late Golgi while Sec7–GFP remains in place under hypo-osmotic shock. mCH–Imh1 was coexpressed with Sec7–GFP in WT cells. Cells were grown to midlog phase in YPD medium. For hypo-osmotic shock treatment, the medium was removed and the cells were suspended in water (with different dilutions of medium as indicated in the figure; 100% indicates a suspension of cells in water) for 5 min. The detailed procedures are described in Methods. **c**, Mislocalized mCH–Imh1 after hypo-osmotic shock treatment is restored by the addition of glycerol-supplemented medium. mCH–Imh1 was coexpressed with Sec7–GFP in WT cells. Cells were grown to midlog phase in YPD medium. For the hypo-osmotic shock treatment, the medium was removed and the cells were suspended in water for 5 min. Then, the cells were suspended in YP or in YP containing 0.1 M glycerol, NaCl, sorbitol or maltose. The ratio of colocalization between Imh1 and Golgi marker Sec7 was quantified (*N* = 3, *n* = 50). PCC, Pearson's correlation coefficient. Data are presented as mean ± s.d. of three independent experiments. NS, not significant. Statistical analysis was conducted using a one-way ANOVA with Dunnett's post hoc multiple-comparison test. The WT strain without treatment was used as a reference. Scale bars, 5 μm.

(ref. [13]). Two response mechanisms that involve Imh1 have been identified to be activated by ER stress. One involves the phosphorylation of Syt1, which activates Arl1 to recruit Imh1 to the Golgi[14]. Another involves the phosphorylation of Imh1 by the MAP kinase Slt2/ERK2, which promotes the role of Imh1 in GARP-mediated retrograde transport to the Golgi[13]. Beyond ER stress, the other major pathologic conditions can affect Imh1 function remain to be identified. An intriguing possibility is suggested by a previous observation that hypo-osmotic-like stress harbored in aneuploidy cells, which is accompanied by greater glycerol efflux, impairs endocytosis[15]. Notably, what transport factors are

targeted in this situation and, at a broader level, what other transport pathways could be affected remain outstanding questions.

Glycerol is known to function as an important osmoprotective molecule during altered osmolarity conditions[16]. It has been shown that hypo-osmotic shock stimulates the activation of the cell wall integrity (CWI) pathway[17]. Moreover, low-osmolarity conditions are known to induce glycerol efflux from cells through the export channel Fps1 (ref. 18).

Glycerol can also act to stabilize protein folding. The mechanism is thought to involve preferential exclusion, which reduces the protein–solvent surface and increases the chemical potential, resulting in proteins adopting more compact structures[19–22]. This effect of glycerol has been illustrated in multiple settings. For instance, glycerol stabilizes protein folding and restores the functional activity of mutant CFTRΔF508, a common variant seen in persons with cystic fibrosis[23]. Glycerol has also been found to protect yeast aldehyde dehydrogenase activity by inducing protein conformation changes that prevent inhibition by trivalent arsenical compounds[24]. Furthermore, glycerol has been shown to protect tropomyosin, a long coiled-coil protein, against thermal and urea denaturation[25].

Glycerol is also well known to participate in cellular metabolic processes, including energy use, lipid synthesis and balance of the nicotinamide adenine dinucleotide (NAD$^+$) redox pool[26]. The most extensively studied mechanism of glycerol production involves reduction of the glycolytic intermediate dihydroxyacetone phosphate (DHAP) into glycerol 3-phosphate (G3P) by G3P dehydrogenase (GPD) and then the dephosphorylation of G3P by G3P phosphatase (GPP) to form glycerol[26]. GPD activity in *Saccharomyces cerevisiae* is encoded by the isogenes *GPD1* and *GPD2*, while *GPP1* and *GPP2* encode isoforms of GPP (ref. 26). In this regard, the potential elucidation of how glycerol affects a transport pathway would also provide a fresh perspective on how one major cellular process (metabolism) can impact another (transport).

In the current study, we find that glycerol promotes the Golgi localization of Imh1. We first establish that hypo-osmotic conditions, which induce glycerol efflux, affect Imh1 localization. We then show more directly that glycerol regulates Imh1 localization. Subsequently, we find that a mammalian golgin is similarly regulated by glycerol. Elucidating how glycerol acts, our results suggest that it affects the conformation of Imh1 to promote Imh1 Golgi localization. These results not only advance the understanding of how golgins are regulated but, because glycerol is well known to act in cellular metabolism, also reveal a connection between cellular metabolism and vesicular transport that has not been appreciated.

Result

Glycerol restores Imh1 localization after hypo-osmotic shock

The cell wall is essential to preserving the integrity of yeast cells during osmotic stress. Yeast that expresses cell wall protein mutations present with a weakened cell wall, which generate a hypo-osmotic stress-like condition[27]. A previous study showed that the glycerol concentration was greatly decreased in cells carrying a mutant form of *wscA*, which is a cell wall sensor in *Aspergillus nidulans*[28]. In yeast, the cell wall sensor is encoded by *WSC1* (ref. 28). We found that Imh1 was released from the Golgi in *wsc1Δ* cells, which was reversed by treatment with a physiological concentration of 0.1 M glycerol[29–31] but not NaCl or sorbitol (Fig. 1a).

To show more directly that hypo-osmotic shock affects Imh1 localization, we next subjected yeast cells to growth medium diluted with varying percentages of water. We observed that, within 5 min in the 80% water dilution, a portion of Imh1 was no longer localized to the Golgi. In pure water (100%), Imh1 was completely cytosolic. In contrast, the distribution of Sec7, which also localizes to the Golgi, was not affected (Fig. 1b). We also examined different Golgi-resident peripheral membrane proteins and we found that they did not become cytosolic in cells treated with hypo-osmotic shock (Extended Data Fig. 1a). We next rescued the water-induced hypo-osmotic shock with different osmolytes and found that the YP medium containing 0.1 M glycerol (YPG) but not NaCl, sorbitol or maltose restored Imh1 localization (Fig. 1c). Thus, these initial results suggest a selective role of glycerol in modulating Imh1 localization.

Reducing glycerol levels impairs Golgi localization of Imh1

We next sought to perturb the glycerol level in cells by targeting its biosynthesis. Gpd1/2 and Gpp1/2 are involved in the glycerol biosynthesis pathway in yeast (Fig. 2a). We found that both Arl1 and Imh1 became cytosolic in *gpd1Δ* and *gpp1/2Δ* cells while Sec7 maintained its Golgi localization (Fig. 2b). We also found that Imh1 localization was not altered in *gpd2Δ* cells, which is explained by a previous finding that Gpd2 is only activated under anaerobic conditions[32]. Moreover, the expression of Gpd1 but not the enzymatically inactive Gpd1-K245A mutant[33] in *gpd1Δ* cells or Gpp2 in *gpp1/2Δ* cells resulted in Imh1 relocalizing to the Golgi (Fig. 2c,d). Furthermore, examining other Golgi-localized peripheral membrane proteins, we found that they did not become cytosolic in *gpd1Δ* and *gpp1/2Δ* cells (Extended Data Fig. 1b). To further investigate whether the regulation of golgin localization by glycerol is selective, we selected two other yeast golgins, Rud3 and Sgm1, the former of which was shown to bind to Arf1 (ref. 34), whereas the latter was shown to be recruited by Rab protein Ypt6 (ref. 35). We found that the localization of Rud3 and Sgm1 in *gpd1Δ* cells remained in Golgi-like puncta, suggesting that glycerol regulation of golgin localization is selective (Extended Data Fig. 1c). These results further support the specificity by which glycerol regulates the Golgi localization of Imh1.

### Glycerol targets Imh1 to affect its Golgi localization

We next sought to elucidate how glycerol affects Imh1 localization. We initially examined whether glycerol targets the key upstream regulator of Imh1 localization, Arl1. Examining *gpd1Δ* and *gpp1/2Δ* cells, we found that Arl1 is cytosolic in these cells (Fig. 2b). Although this finding seemingly indicated that glycerol regulates Imh1 localization through Arl1, a caveat was that Imh1, upon being recruited to the Golgi by Arl1, inhibits Gcs1, the GAP that deactivates Arl1 (ref. 12), which serves to promote the Golgi localization of both Arl1 and Imh1 (ref. 13) (Extended Data Fig. 2a). Moreover, our previous study showed that accumulation of highly activated Arl1–GTP at the Golgi in the gcs1-deleted mutant

Fig. 2 | Glycerol synthesis is required for proper Arl1 and Imh1 localization. **a**, Glycerol synthesis pathway in *S. cerevisiae*. The glycolytic metabolite DHAP is converted to G3P by GPD1 and GPD2 and glycerol is then produced by the phosphatases GPP1 and GPP2 (ref. 26). **b**, Arl1 and Imh1 were mislocalized in *gpd1Δ* and *gpp1/2Δ* cells. Deletion of the upstream Arl1 regulator Arl3 and the Arl1 guanine-nucleotide exchange factor Syt1 resulted in mislocalization of Arl1 and Imh1. mCH–Imh1 or Arl1–mRFP was coexpressed with Sec7–GFP in the indicated strains. Live cells were observed in midlog phase. Scale bars, 5 μm. In **a**,**b**, the ratio of colocalization between Imh1 or Arl1 and Golgi marker Sec7 was quantified (*N* = 3, *n* = 50). The data are presented as the mean ± s.d. of three independent experiments. Statistical analysis was conducted using a one-way ANOVA with Dunnett's post hoc multiple-comparison test. The WT strain was used as a reference. **c**,**d**, Gpd1 and Gpp1/2 regulate the localization of Imh1. **c**, The enzymatic activity of Gpd1 is required for proper Imh1 localization. mCH–Imh1, Sec7–GFP and Gpd1 constructs were coexpressed in cells (Gpd1-K245A, enzymatically inactive Gpd1 mutant). **d**, Gpp1/2 are required for Imh1 proper localization. mCH–Imh1, Sec7–GFP, and Gpp2 constructs were coexpressed in cells. Live cells were observed in the midlog phase. The numbers of mCH–Imh1 puncta were determined with ImageJ Fiji software (*N* = 3, *n* = 50). Data are presented as the mean ± s.d. of three independent experiments. Statistical analysis was conducted using a one-way ANOVA with Dunnett's post hoc multiple-comparison test. The WT strain was used as a reference. Scale bars, 5 μm.
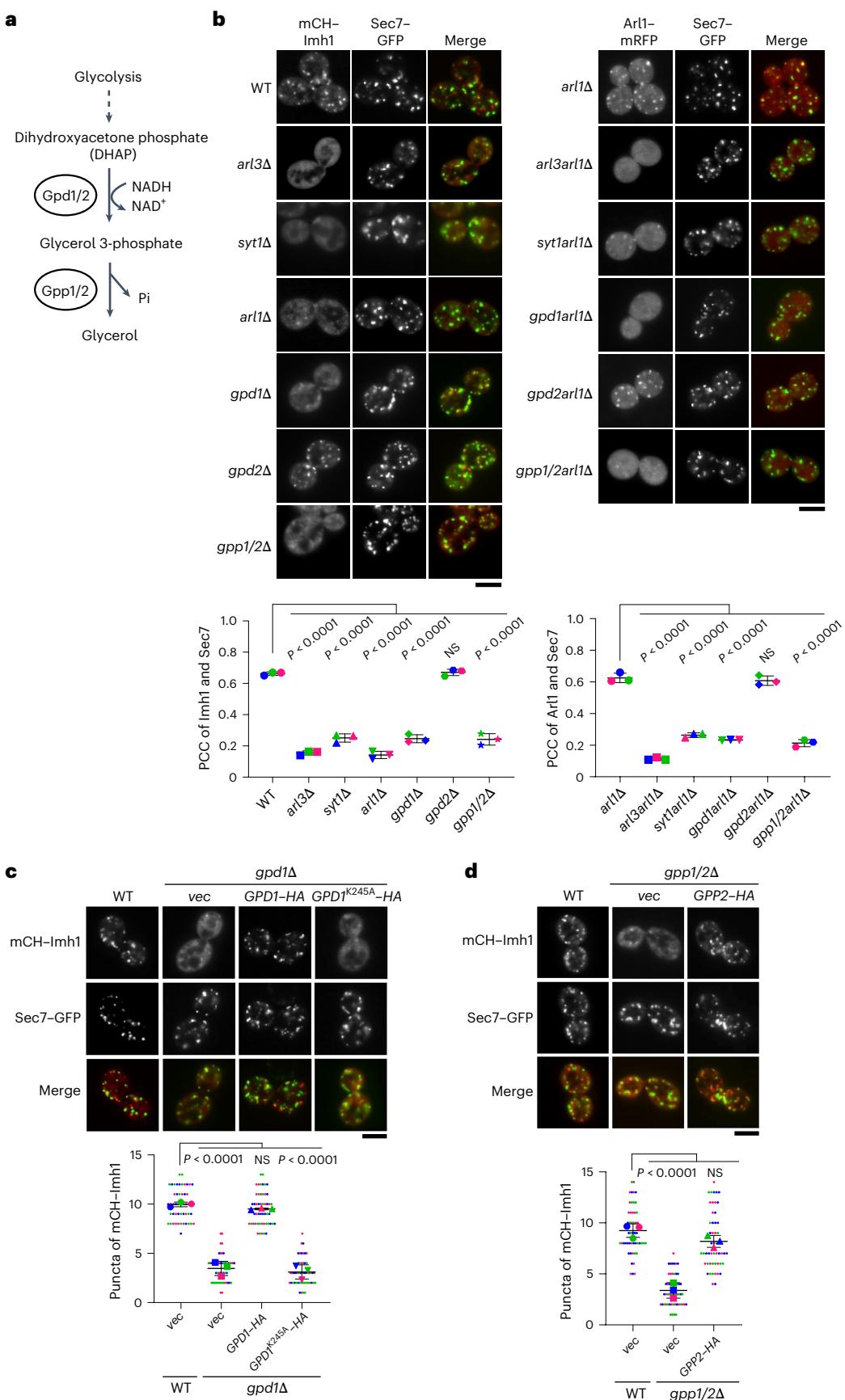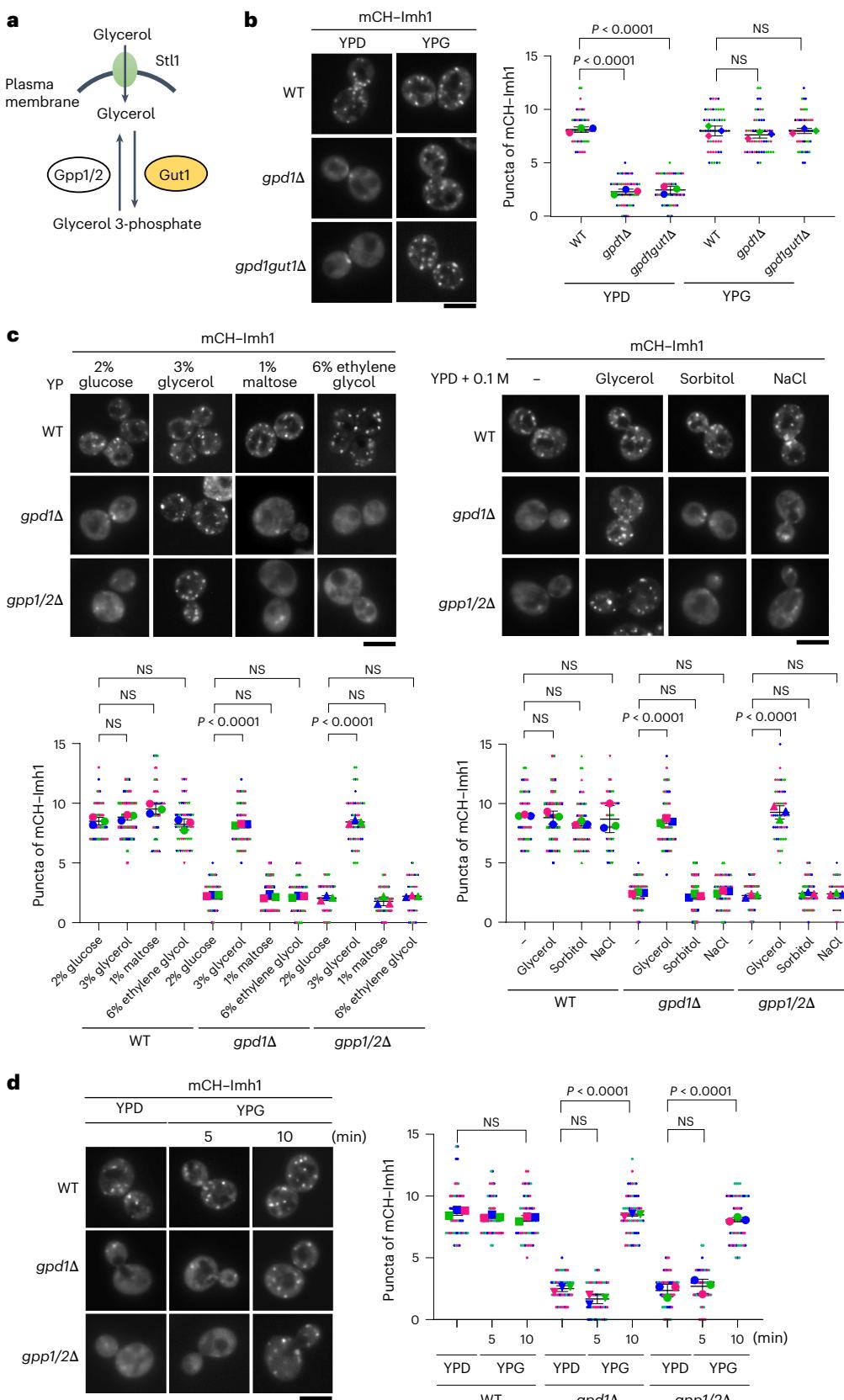
constitutively enhances the flippase activity of Drs2, leading to an increase in abnormal high membrane curvature and, thus, dissociation of Imh1 from the Golgi membrane[36]. As such, cytosolic Arl1 seen in *gpd1*Δ cells could be because of Imh1 being directly targeted by glycerol deficiency, resulting in Imh1 not being present at the Golgi to prevent the

GAP activity of Gcs1. To sort out between the two possibilities, we next examined the localization of Arl1 in *gpd1gcs1*Δ cells. We found that the Golgi localization of Arl1 was maintained in both *gcs1*Δ and *gpd1gcs1*Δ cells, and notably, Imh1 was cytosolic (Extended Data Fig. 2a, b). Thus, this result suggested that glycerol does not regulate Imh1 through

Fig. 3 | Glycerol serves as an osmolyte that regulates Imh1. a, Model of glycerol transport into yeast cells and the glycerol metabolism for G3P production. Glycerol enters yeast cells through the Stl1 channel and is then phosphorylated by Gut1 to produce G3P, which is the substrate of Gpp1/2 (ref. 26). **b**, Glycerol restores mislocalized Imh1 independent of Gut1. Cells expressing mCH–Imh1 were grown to midlog phase in YPD medium, the medium was removed and the cells were suspended in YPG for 10 min. Scale bar, 5 μm. **c**, Glycerol specifically rescues the Imh1 localization in glycerol-deficient cells. mCH–Imh1 was expressed in cells. Cells were grown to midlog phase in YPD medium, the medium was removed and the cells were suspended in YP medium with 2% glucose, 3% glycerol, 1% maltose or 6% ethylene glycol or in YPD medium with 0.1 M glycerol, NaCl or sorbitol. Scale bars, 5 μm. **d**, Glycerol rescues the localization of Imh1 in *gpd1Δ* and *gpp1/2Δ* cells within 10 min. Cells expressing mCH–Imh1 were grown to midlog phase in YPD medium, the medium was removed and the cells were suspended in YP medium containing 0.1 M glycerol. mCH–Imh1 was observed after glycerol rescue for 5 and 10 min. Scale bar, 5 μm. **b–d**, The numbers of mCH–Imh1 puncta were determined with ImageJ Fiji software (*N* = 3, *n* = 50). Data are presented as the mean ± s.d. of three independent experiments. Statistical analysis was conducted using a one-way ANOVA with Dunnett's post hoc multiple-comparison test.

Arl1. We also found that the constitutively active mutant Arl1^{QL} localized to the Golgi in *gpd1Δ* cells (Extended Data Fig. 2c), suggesting that glycerol deficiency does not alter the ability of the Golgi membrane to support Arl1 localization. Furthermore, as Arl3 is needed for Arl1 localization to the Golgi[37], we found that Arl3 localizes to the Golgi in the glycerol-deficient cells (Extended Data Fig. 2d). Thus, these results rule out key upstream regulators of Imh1 being targeted by glycerol in explaining how it regulates Imh1 localization.

We next examined whether glycerol could affect Imh1 indirectly through another mechanism. Arl1, Gea2 and Drs2 are known to form a complex and cooperate in regulating Golgi membrane curvature[9]. By altering the lipid curvature environment, Drs2 facilitates the targeting of Gcs1 to the Golgi to promote Arl1 deactivation[36]. Thus, because the loss of Drs2 activity leads to Imh1 release from the Golgi[9,36], we asked whether cytosolic Imh1 seen in glycerol-deficient cells could be because of impaired Drs2 activity. Drs2 abrogation results in hypersensitivity to the PE-binding peptide cinnamycin[38,39]. We found that *drs2Δ* but not *gpd1Δ* cells showed delayed growth after 6 h of cinnamycin treatment (Extended Data Fig. 3a). Moreover, we found that glycerol failed to restore Imh1 localization to the Golgi in *drs2Δ* cells (Extended Data Fig. 3b). These results suggest that the lack of glycerol in *gpd1Δ* cells does not alter Drs2 flippase activity and that glycerol serves as a distinctive regulator of Imh1 localization independent of Drs2. We also considered that glycerol might be metabolized to other lipid derivatives[40]. Thus, we confirmed that phospholipid-binding proteins did not become cytosolic in the glycerol-deficient mutant cells (Extended Data Fig. 4).

We then explored yet another way that glycerol can indirectly affect Imh1. Glycerol enters yeast cells through the import channel Stl1 and then becomes phosphorylated by Gut1 to generate G3P, a key intermediate in glucose and lipid metabolism[26] (Fig. 3a). Thus, to determine whether Imh1 localization can be regulated by the metabolites of glycerol, we examined *gpd1gut1Δ* cells. We found that glycerol rescued the Golgi localization of Imh1 in these cells (Fig. 3b), thus ruling against glycerol metabolites mediating the regulation of Imh1 by glycerol. We further examined whether defects in glycerol transporters, Stl1 influx channel and Fps1 efflux channel, could affect Imh1 localization and observed that Imh1 was mislocalized in *stl1Δ* and *fps1Δ* cells. We also found that the mislocalization of Imh1 could be restored in *stl1Δ* and *fps1Δ* cells by expression of Stl1 and Fps1, respectively (Extended Data Fig. 5a), but not in YPG (Extended Data Fig. 5b). These results suggest that the effect of Stl1 and Fps1 glycerol transport channel on Imh1 localization may involve other signals or functions mediated by Stl1 and Fps1 (refs. 41–43).

We also examined the ability of different carbon sources, such as maltose and ethylene glycol, or osmotic stress inducers, including sorbitol and sodium chloride, in restoring the Golgi localization of Imh1 in *gpd1Δ* and in *gpp1/2Δ* cells. Only glycerol rescued the Golgi localization of Imh1 in these glycerol-deficient cells (Fig. 3c), which occurred within 10 min of its feeding (Fig. 3d). Thus, these results further support that glycerol directly regulates Imh1 to promote its Golgi localization. Overall, our data indicate that glycerol likely acts directly on Imh1 to affect its Golgi localization.

## Glycerol regulates Imh1 conformation for Golgi localization

We next sought to elucidate how glycerol directly affects Imh1. Golgins need to undergo self-interaction for their localization to the Golgi[44]. In the case of Imh1, we previously found that a truncated form of Imh1 that cannot undergo self-interaction fails to localize to the Golgi[12]. However, tagging this mutant construct with DsRed, a fluorophore that tetramerizes, resulted in the chimeric mutant localizing to the Golgi[12]. Led by this consideration, we next found that DsRed tagging could restore the Golgi localization of not only full-length Imh1 in glycerol-deficient cells but also truncation mutants Imh1-C177 and Imh1-C89 (Fig. 4a). Moreover, glycerol restored the Golgi localization of Imh1-C177 in *gpd1Δ* and *gpp1/2Δ* cells (Fig. 4b). These results suggest that the self-interaction property of Imh1 may be regulated by glycerol.

To dissect whether Imh1 dimerization is altered in glycerol-deficient cells, we performed coimmunoprecipitation (co-IP) to examine Imh1 self-dimerization in wild-type (WT) and *gpd1Δ* cells. However, we found that Imh1 self-interaction showed no difference in *gpd1Δ* cells compared to WT cells using co-IP experiments (Extended Data Fig. 6a). To gain further insight into what this property may be, we next pursued the purification of Imh1 for direct examination. We initially tried to purify full-length Imh1 by gel filtration chromatography and found that it was aggregated upon cell lysis (Extended Data Fig. 6b). A way to overcome this hurdle was suggested by a previous observation that C-terminal constructs of Imh1 that retain both the GRIP domain and the third coiled-coil domain could still localize to the Golgi when expressed in cells[12]. Thus, we subjected one such Imh1 construct (Imh1-C213) to purification by gel filtration. The result showed that Imh1-C213 did not elute at the expected position for a dimer (Extended Data Fig. 6c). A previous study suggested that Imh1 may possess an extended shape[44]; thus, the elution behavior of nonglobular proteins in gel filtration may not accurately represent their molecular weight. To address this issue, we performed sedimentation velocity analysis and observed the 54.4 kDa of Imh1-C213 with a sedimentation coefficient 2.8 S, confirming that Imh1-C213 forms

Fig. 4 | Forced tetramerization led to Imh1 relocalization to the *trans*-Golgi in glycerol-deficient *gpd1Δ* and *gpp1/2Δ* cells. a, DsRed-tagged Imh1 restored Imh1 mislocalization in glycerol-deficient cells. mCH-tagged or DsRed-tagged Imh1, Imh1-C177 or Imh1-C89 was expressed in *gpd1Δ* and *gpp1/2Δ* cells. **b**, Glycerol restored mislocalized Imh1-C177 in *gpd1Δ* and *gpp1/2Δ* cells. mCH–Imh1-C177 was coexpressed with Sec7–GFP in WT, *gpd1Δ* and *gpp1/2Δ* cells. Cells were grown to midlog phase in YPD medium, the medium was removed and the cells were suspended in YP medium with 0.1 M glycerol for 10 min. **c**, GFP-tagged or TurboRFP-tagged Imh1 cannot restore Imh1 mislocalization in glycerol-deficient cells. TurboRFP-tagged or GFP-tagged Imh1 was coexpressed with Sec7–GFP or Sec7–mRFP in WT, *gpd1Δ* and *gpp1/2Δ* cells. In **a–c**, live cells were observed in the midlog phase. In **a**, the numbers of mCH–Imh1 puncta were determined with ImageJ Fiji software (*N* = 3, *n* = 50). The data are presented as the mean ± s.d. of three independent experiments. Statistical analysis was conducted using a one-way ANOVA with Dunnett's post hoc multiple-comparison test. Scale bars, 5 μm. In **b,c**, the ratio of colocalization between Imh1 and Golgi marker Sec7 was quantified (*N* = 3, *n* = 50). The data are presented as the mean ± s.d. of three independent experiments. Statistical analysis was conducted using a one-way ANOVA with Dunnett's post hoc multiple-comparison test. Scale bars, 5 μm.

a dimer (Extended Data Fig. 6d). Size-exclusion chromatography with multiangle static light scattering (SEC–MALS) and mass photometry were also used to reanalyze the Imh1-C213 molecular weight and indicated that it indeed forms a dimer (Extended Data Fig. 6e,f). As further

confirmation for the importance of the strength of Imh1 self-interaction, we examined the effect of dimerizing Imh1 constructs through tagging at the N terminus with either GFP or TurboRFP, which induces stronger dimerization[45], and found that neither tag could restore Imh1 localization
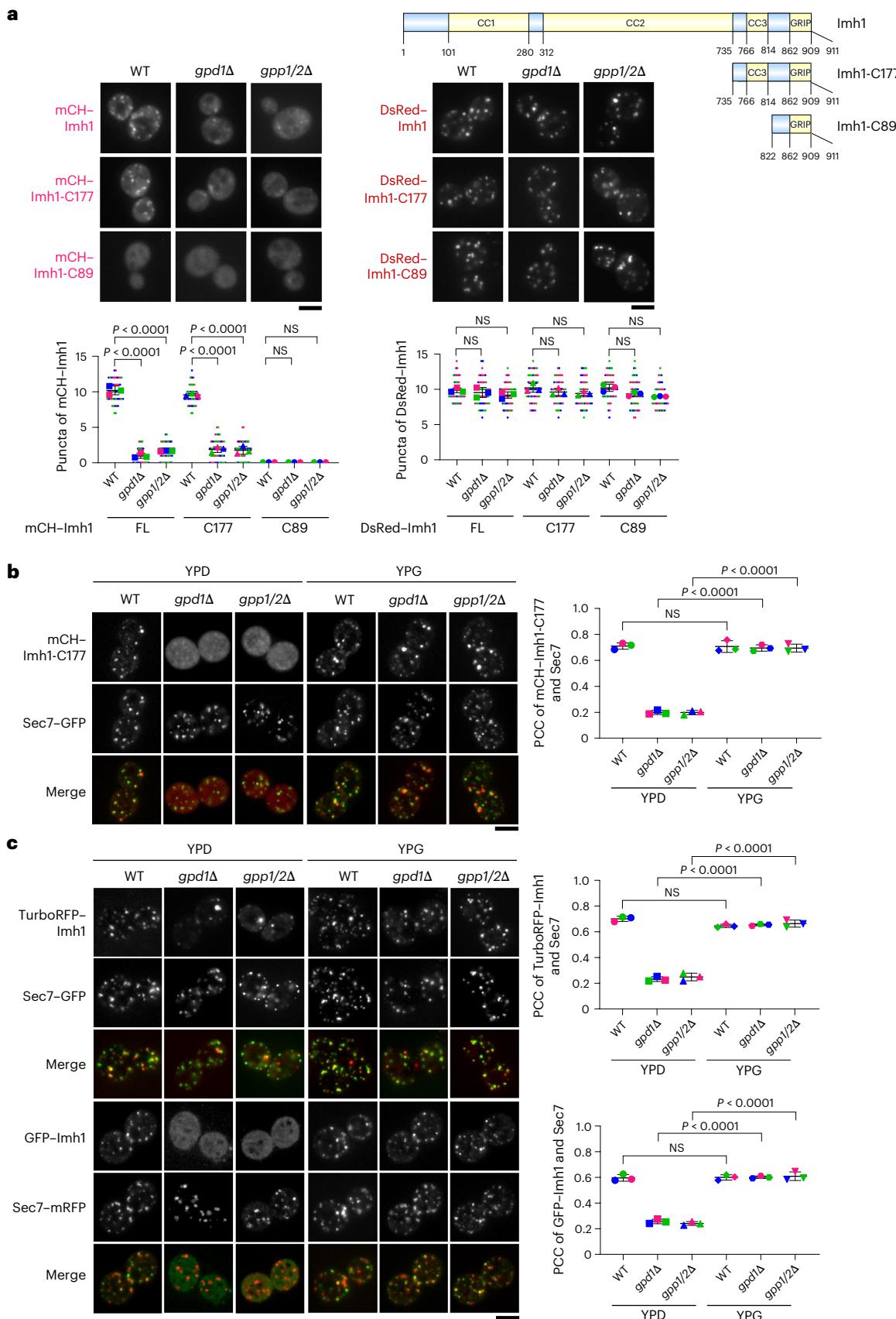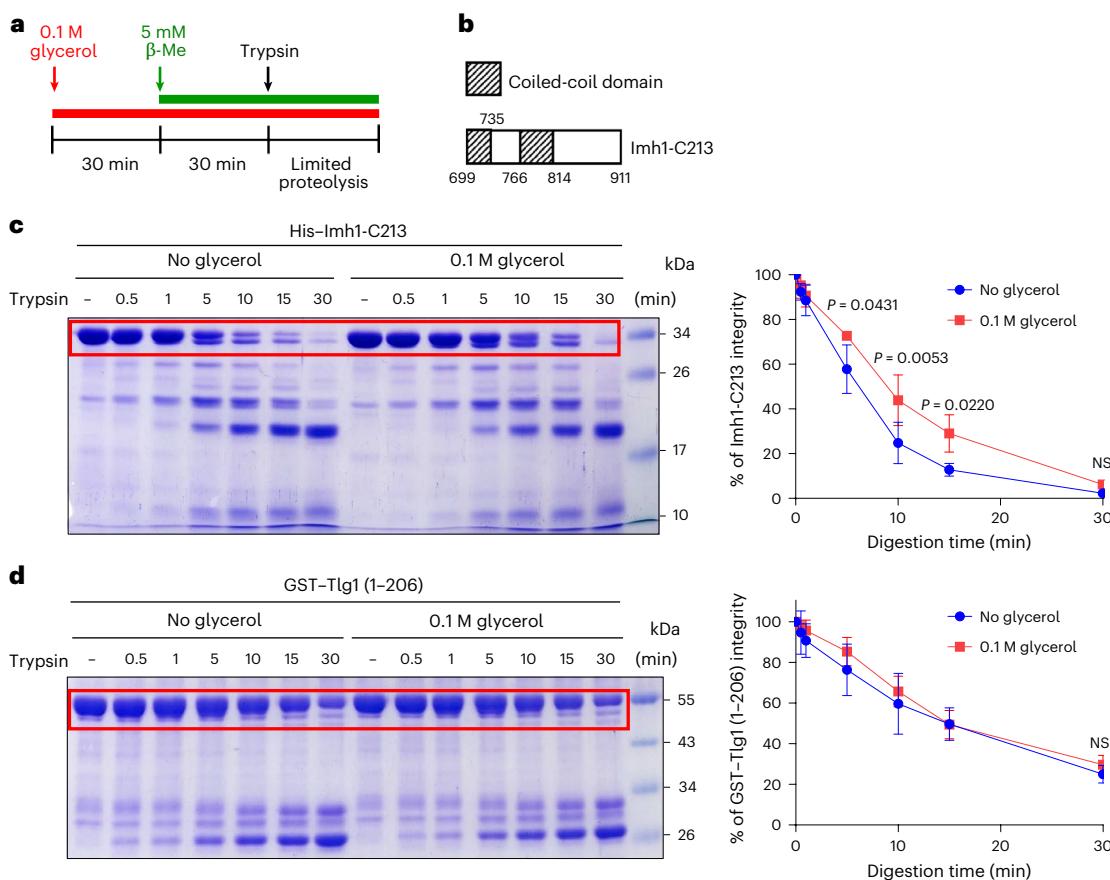
Fig. 5 | Glycerol attenuates proteolysis of Imh1 C-terminal fragment in vitro.
a, Schematic diagram of glycerol preincubation conditions and trypsin limited proteolysis. Recombinant purified His-tagged Imh1-C213 fragment (C-terminal 699–911 residues) or Tlg1 (1–206) from *E. coli* was first preincubated with 0.1 M glycerol for 30 min at 30 °C before adding 5 mM β-mercaptoethanol (β-Me) for an additional 30 min. The pretreated proteins were then digested with trypsin (trypsin-to-protein ratio of 1:20 w/w) on ice for the time indicated. **b**, Schematic diagram of coiled-coil domain in golgin Imh1-C213 fragment. **c**, Glycerol treatment attenuates recombinant Imh1-C213 trypsin proteolysis in vitro.

d, Glycerol treatment does not protect recombinant Tlg1 (1–206) protein from trypsin-based proteolysis in vitro. **c**,**d**, The protein bands in the cropped regions (red rectangle) were quantified. The signals of protein bands were determined using ImageJ Fiji software (*N* = 3). At the time point of 30 min, the protein bands with the trypsin digestion were normalized to the uncut protein bands and the percentage of remaining proteins was calculated. The data are presented as the mean ± s.d. of three independent experiments. Statistical analysis was conducted using a two-way ANOVA. The uncut protein was used as a reference.

in glycerol-deficient cells (Fig. 4c). These results are consistent with our observation above that the impaired Golgi localization of Imh1 constructs seen in glycerol-deficient cells could be corrected by DsRed tagging that could induce much stronger self-interaction of Imh1.

Glycerol affects the conformation of Imh1 in vitro
To examine for a more subtle effect of glycerol on Imh1 structure, we next pursued limited proteolysis. Glycerol (up to about 1.4 M) was found previously not to interfere trypsin proteolytic activity[46]. Performing limited proteolysis using trypsin (Fig. 5a), we found that a general physiological concentration of glycerol (0.1 M) moderately attenuated the ability of trypsin to degrade the Imh1-C213 construct (Fig. 5b,c). For comparison, we found that glycerol has no effect on the limited proteolysis of the t-SNARE protein Tlg1 (1–206), an N-terminal domain with a three-helix bundle[47] (Fig. 5d). This result suggests that the conformation of Imh1 can be influenced by glycerol in this assembled state. It is known that changes in the emission spectra of tryptophan are because of conformational changes of the protein, association of subunits, ligand binding or denaturation, which affect the local environment of the indole ring[48]. We also used Imh1-C213, which contains a tryptophan at the 59th residue, to perform the tryptophan fluorescence assay and found that glycerol increases the intensity of tryptophan fluorescence in Imh1-C213 (Extended Data Fig. 7 and Supplementary Fig. 1).

To gain structural insights into the effects of glycerol on Imh1 conformation, we conducted a triplicate label-swap quantitative proteomics analysis using isotope-labeled (nondeuterated (d_0) and deuterated (d_4)) bis(sulfosuccinimidyl)suberate (BS3) crosslinkers, combined with liquid chromatography–tandem mass spectrometry (LC-MS/MS), to identify and quantify the ratios of differentially crosslinked peptides on Imh1-C213 in both the absence and the presence of glycerol (Fig. 6a). A total of 13 crosslinks were consistently detected across all six experiments (Supplementary Table 1 and Supplementary Fig. 2). To evaluate the impact of glycerol on conformational changes in Imh1, we selected crosslinks that exhibited consistent regulatory trends and calculated their mean glycerol-to-control ratios. The results revealed that the abundance of six crosslinks changed, ranging from 7% to 16%, indicating that glycerol influences the crosslinking pattern of Imh1-C213 (Fig. 6b, Extended Data Fig. 8 and Supplementary Table 1). Thus, findings from direct examinations of Imh1 using in vitro assays, including limited proteolysis, tryptophan fluorescence and crosslinking MS, all suggest that glycerol affects the conformation of Imh1.

Ethanol antagonizes Imh1 localization promoted by glycerol
In considering how glycerol could affect Imh1 conformation, we noted that glycerol was found to stabilize proteins by changing the energetics of hydrophobic interactions and shifting the native protein toward
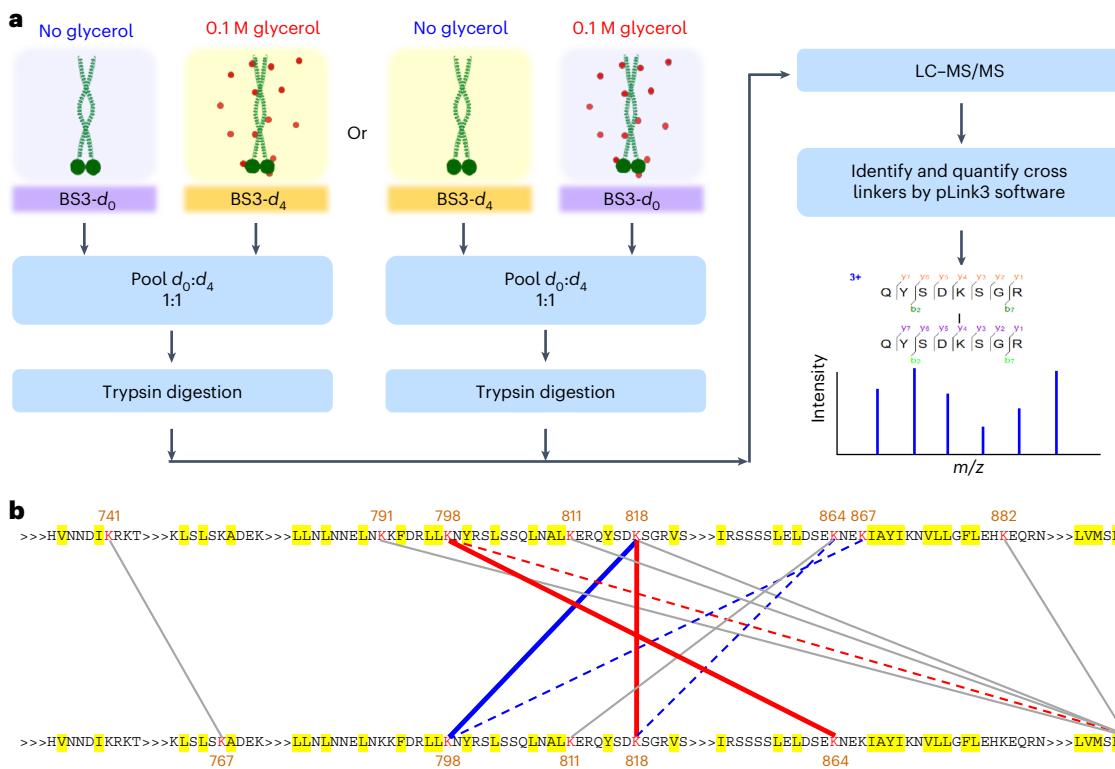
Fig. 6 | Identification and quantification of potential interaction sites of Imh1-C213 by isotope-labeled crosslinkers and MS. a, Schematic representation of the workflow of crosslinking MS analysis with or without glycerol treatment. The purified His-tagged Imh1-C213 fragment (C-terminal 699–911 residues) was first preincubated with or without 0.1 M glycerol and then crosslinked with equimolar amounts of d_0 or d_4 BS3. The crosslinking step was repeated with an exchange of labels. Equal amounts of light (d_0) and heavy (d_4) crosslinked proteins were pooled and subjected to trypsin digestion and LC–MS/MS analysis. The crosslinked peptides were identified and quantified using the pLink3 software. The detailed procedure is described in Methods. **b**, Map of potential crosslinked sites in His–Imh1-C213 dimer in the absence or presence of 0.1 M glycerol. A total of 13 crosslinked peptide pairs, consistently detected all across six experiments, each supported by at least one spectrum match with a pLink3 spectrum score > 0.85 in every experiment, are presented. The

crosslinked lysine residues are represented by connecting lines in different colors on the basis of quantified ratios (glycerol to control). Six crosslinks displayed consistent regulatory trends in at least three of the six quantified ratios, with mean glycerol-to-control ratios of >1.05 or <0.95. Specifically, crosslinks with increased abundance after glycerol treatment are represented by red lines (solid for ratios ≥ 1.1; dashed for ratios between 1.1 and 1.05), while those with decreased abundance are shown in blue (solid for ratios ≤ 0.90; dashed for ratios between 0.90 and 0.95). Crosslinks that do not meet these criteria are displayed in gray. Potential hydrophobic regions in the amino acid sequence are highlighted in yellow. The crosslinked sites and their peptide sequences in the map are listed in Supplementary Table 1. The MS data were deposited to the ProteomeXchange consortium through the PRIDE partner repository with the dataset identifier PXD061125.

more compact conformations[19]. In contrast, ethanol was suggested to disrupt the hydrophobic interactions to impair protein folding[49,50]. Thus, we assessed whether ethanol antagonizes the ability of glycerol to promote Imh1 localization. We first confirmed that different Golgi-resident peripheral membrane proteins did not become cytosolic in cells treated with 3% ethanol (Extended Data Fig. 1a). We found that this was indeed the case, as the Golgi localization of Imh1 observed in cells cultured in YPG became disrupted when ethanol was also added (Fig. 7a). However, ethanol had no effect on DsRed–Imh1 localization in YP medium and YPG medium, suggesting that forcing a stronger self-interaction of Imh1 by tagging with DsRed suppresses the effect of ethanol. Moreover, the cytosolic distribution of Imh1 induced by ethanol could be reversed by transferring cells that were cultured in YP medium supplemented with ethanol to YPG medium (Fig. 7b). Collectively, these results support that glycerol affects the conformation of Imh1 by targeting hydrophobic surface regions.

Glycerol aids Imh1-mediated SNARE transport under ER stress
We next assessed the functional consequence of glycerol-mediated regulation of Imh1. We previously demonstrated that Imh1 but not Arl1 acts as a direct mediator of GARP-dependent retrograde transport of SNAREs (Snc1 and Tlg1) to the Golgi under tunicamycin (TM)-induced

ER stress[13]. Because glycerol is required for Imh1 localization, we examined the effect of glycerol deficiency during ER stress by assessing SNARE trafficking in *gpd1Δ* cells. We first found that Snc1 and Tlg1 were mislocalized in *gpd1Δ* cells after TM treatment and this effect was phenocopied in *imh1Δ* cells (Fig. 8a). We next observed that the mislocalized Snc1 was rescued upon glycerol addition (Fig. 8b). Furthermore, the localization of Imh1 was restored after glycerol addition under TM-induced stress (Extended Data Fig. 9). These results confirmed that the effect of glycerol on Imh1 localization also affects its role in retrograde transport to the Golgi.

Glycerol supports golgin-mediated Golgi integrity in cells
To examine whether the regulation of GRIP domain-containing golgins by glycerol also occurs in mammalian cells, we next examined golgin 245 (p230), which also depends on the recruitment of Arl1 for Golgi targeting[5]. Upon knocking down the Gpp1/2 human homolog G3P phosphatase (PGP) in HeLa cells, we found that p230 staining became more diffuse (Extended Data Fig. 10a). We also tracked the Golgi membrane by examining B4GALT1 and found that the distribution of this transmembrane Golgi marker also became diffuse (Extended Data Fig. 10a), which is consistent with golgins having a critical role in Golgi integrity. The targeting specificity of these effects was supported
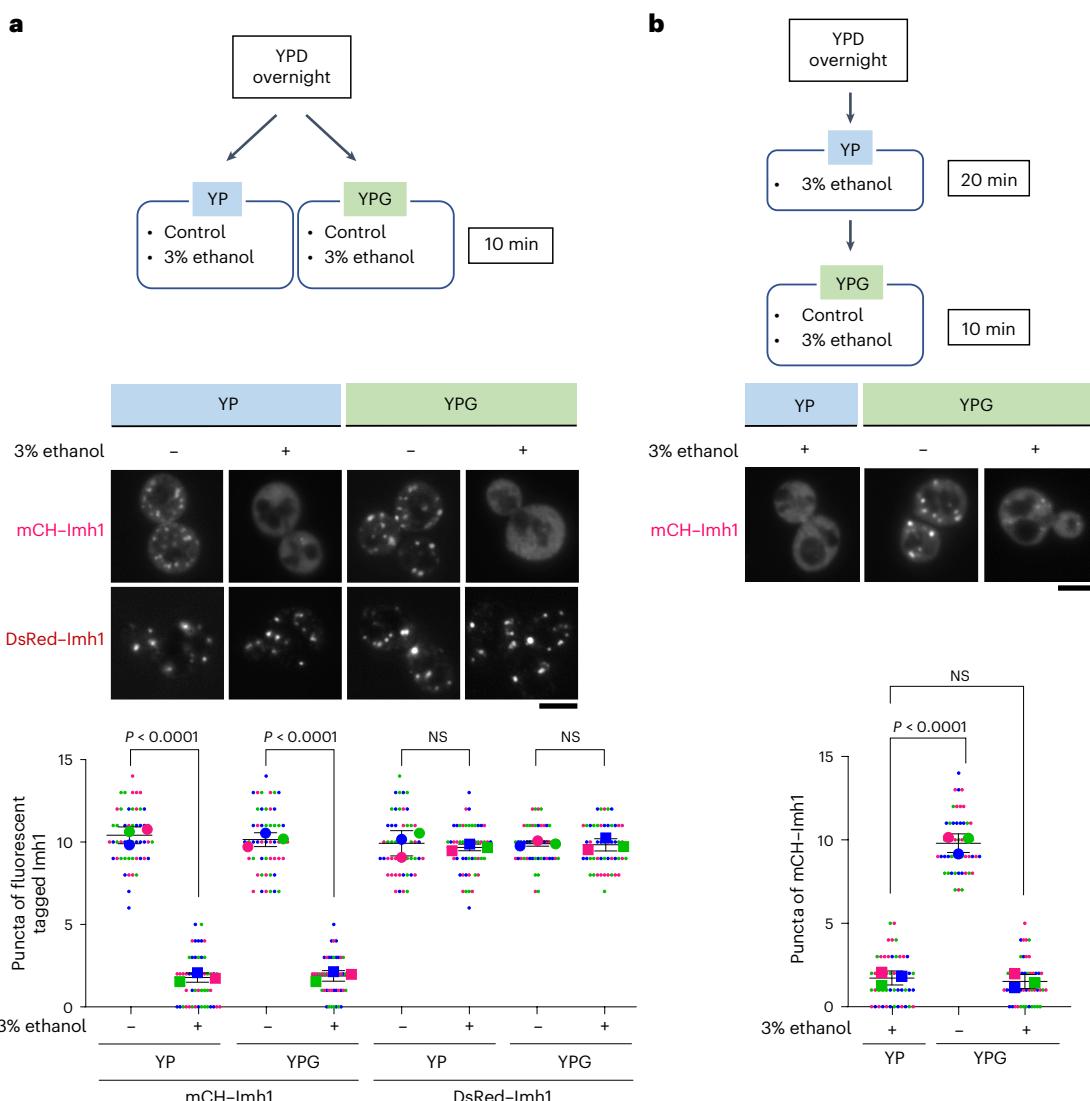
Fig. 7 | Ethanol competes with the function of glycerol in rescuing the localization of Imh1. a, Ethanol affects the mCH–Imh1 Golgi localization in YP and YPG medium. mCH–Imh1 or DsRed–Imh1 was expressed in WT cells. Live cells were cultured to midlog phase in YPD medium. Then, the medium was removed and the cells were suspended in YP medium with or without 3% ethanol or YP medium with 0.1 M glycerol with or without 3% ethanol for 10 min. Scale bar, 5 μm. **b**, Imh1 was mislocalized in the medium supplemented with ethanol. The cells in YP medium with 3% ethanol for 20 min were then suspended in YP with 0.1 M glycerol and 3% ethanol or without ethanol. Scale bar, 5 μm In **a**,**b**, the numbers of mCH–Imh1 puncta were determined with ImageJ Fiji software ($N = 3$, $n = 50$). The data are presented as the mean ± s.d. of three independent experiments. Statistical analysis was conducted using a two-sided unpaired *t*-test (**a**) or one-way ANOVA with Dunnett's post hoc multiple-comparison test (**b**).

by two different small interfering RNA (siRNA) sequences. We then added 0.1 M glycerol and found that the Golgi localization of p230 was restored (Extended Data Fig. 10a). In the siRNA control, we also excluded the effect of glycerol on the localization of the Golgi marker B4GALT1 (Extended Data Fig. 10b). Thus, glycerol also promotes the Golgi localization of a mammalian golgin.

Discussion

Studying Imh1, a prototypic yeast golgin, we discovered that glycerol promotes its Golgi localization, a process critical for its role in vesicular transport and Golgi maintenance. We initially found that the different ways of reducing the cellular level of glycerol all led to Imh1 being released from the Golgi to the cytosol. Subsequently, to elucidate how glycerol regulates Imh1 localization, we explored the different ways that glycerol can act. These include the possibilities that glycerol affects Arl1 localization or the Golgi membrane by targeting Drs2 activity or through metabolites of glycerol. Having ruled out these possibilities,

we then sought to elucidate how glycerol can target Imh1 directly. For this goal, we purified a minimal construct of Imh1 that was previously shown to target to the Golgi properly when expressed in cells and found that it exists as a dimer, supporting a previous model for GRIP domain proteins as extended rod-like homodimeric molecules with a highly asymmetric shape. We then found that, rather than affecting this oligomeric state of Imh1, glycerol exerts a more subtle effect on Imh1, impacting its conformation.

Previous studies have suggested how glycerol can affect protein conformation[19–21,51,52]. One mechanism involves glycerol being preferentially excluded from the surface of proteins[19,20]. Because this exclusion is thermodynamically unfavorable, protein self-association is increased by a decrease in the protein–solvent surface[19,20]. Thus, the reduction in the interface between a protein and solvent renders the system thermodynamically favorable[19,20]. In this regard, ethanol has been suggested to act oppositely in disrupting the hydrophobic interactions to impair protein folding[49,50]. Led by these considerations, we found that ethanol
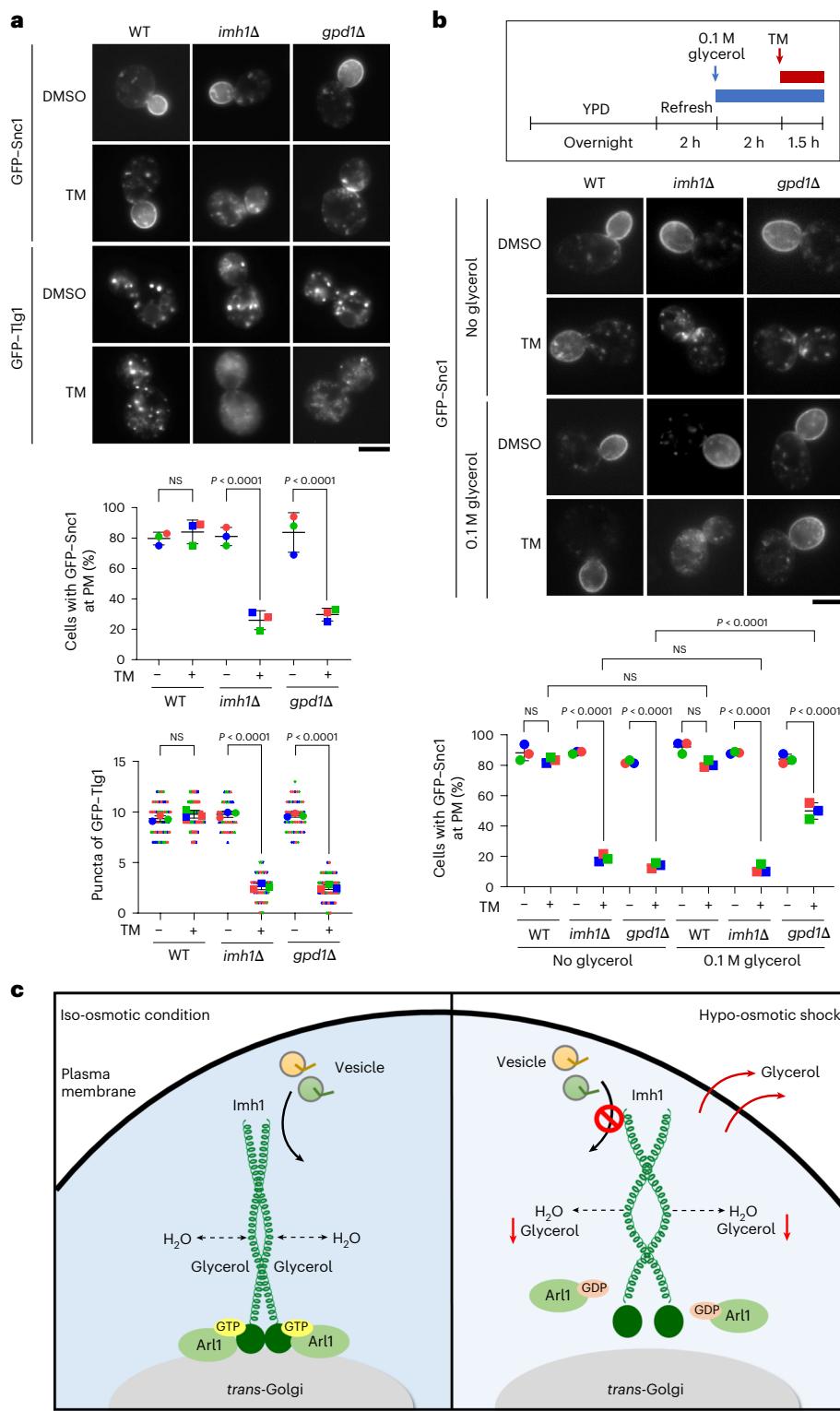
Fig. 8 | Glycerol rescues mislocalized GFP–Snc1 in *gpd1*Δ cells under TM-induced ER stress. a, The distributions of Snc1 and Tlg1 were altered in *gpd1*Δ cells under TM treatment. GFP–Snc1 or GFP–Tlg1 was expressed in WT, *imh1*Δ and *gpd1*Δ cells. Live cells were cultured to midlog phase and treated with 1 μg ml⁻¹ TM for 2 h before observation using fluorescent microscopy. Scale bar, 5 μm. **b**, Glycerol is essential for restoring the distribution of Snc1 in *gpd1*Δ cells under TM treatment. Cells expressing GFP–Snc1 were cultured to midlog phase in YPD medium, 0.1 M glycerol was added and then cells treated with 1 μg ml⁻¹ TM for 1.5 h. No glycerol addition was used as a reference. Scale bar, 5 μm. In **a**,**b**, GFP–Snc1 signals at the plasma membrane (PM) or GFP–Tlg1 puncta were quantified

($N = 3$, $n = 50$). The data are presented as the mean ± s.d. of three independent experiments. Statistical analysis was conducted using a two-sided unpaired *t*-test (**a**) or one-way ANOVA (**b**). **c**, Model of how glycerol regulates golgin Imh1 localization. Under iso-osmotic conditions, a proper glycerol level assists in maintaining Imh1 Golgi localization by fine-tuning the conformation of the coiled-coil region, which in turn stabilizes Arl1–Imh1 Golgi localization. However, under hypo-osmotic shock conditions, glycerol leakage leads to Imh1 loss of conformation and mislocalization from the Golgi, resulting in Arl1 dissociation from the Golgi.

antagonizes Imh1 localization promoted by glycerol. Thus, this result suggests that glycerol likely interacts with hydrophobic surface regions of Imh1 and shifts the native Imh1 to more compact conformations.

In addition to elucidating how glycerol affects Imh1 localization, our findings deepen our understanding of how Imh1 needs to be assembled for its Golgi localization. The Golgi localization of mammalian golgins is thought to be mediated by dimerization of the GRIP domain[5]. However, we found previously that the Golgi localization of the yeast Imh1 requires not only the GRIP domain but also an adjacent coiled-coil domain[12]. This finding raises the possibility that the assembly state of Imh1 needed for its localization may not only involve dimerization. Support that this assembly state likely mediates Imh1 localization comes from further results that the Golgi localization of Imh1, which becomes impaired in glycerol-deficient cells, is restored by tagging Imh1 with DsRed, which assembles as a tetramer at the N terminus[53]. In contrast, tagging Imh1 with fluorophores that induce dimerization at the N terminus of Imh1 does not restore its Golgi localization in glycerol-deficient cells. We reason that tetrameric Imh1 at the N terminus may lead to much stronger self-interaction of Imh1, thereby suppressing the conformational change caused by glycerol deficiency in yeast cells.

We also extended our discovery by showing that glycerol regulates the Golgi localization of a mammalian golgin, p230. Consistent with mammalian golgins acting to promote Golgi integrity[1], we found that Golgi integrity was disrupted when knocking down PGP, the human homolog of yeast Gpp1/2. Moreover, adding glycerol restored both Golgi integrity and p230 localization. Thus, glycerol appears to have an evolutionarily conserved role in regulating the golgins.

In summary, we achieved an enhanced understanding of how Imh1 is regulated and also identified a major pathologic condition, other than ER stress, that affects Imh1 function, which in this case involves hypo-osmotic shock that reduces the cellular glycerol level. Moreover, because glycerol is an intermediate in cellular metabolism, we revealed a connection between intracellular metabolism and transport that has not been appreciated.

Our findings also suggest a working model of how intracellular glycerol regulates the Golgi localization of Imh1 (Fig. 8c). Under iso-osmotic conditions, glycerol targets hydrophobic surface regions of Imh1 and can strengthen hydrophobic interactions in the dimer backbone of Imh1. A reduction in glycerol level under hypo-osmotic stress conditions or when glycerol production is defective alters the effect on the energetics of hydrophobic interactions on self-interacting Imh1 conformation. These changes lead to destabilization of Imh1, which promotes the GAP activity of Gcs1 to deactivate Arl1, resulting in both Arl1 and Imh1 being released from the Golgi complex.

Online content

Any methods, additional references, Nature Portfolio reporting summaries, source data, extended data, supplementary information, acknowledgements, peer review information; details of author contributions and competing interests; and statements of data and code availability are available at https://doi.org/10.1038/s41594-025-01600-x.

References

1. Klumperman, J. Architecture of the mammalian Golgi. *Cold Spring Harb. Perspect. Biol.* **3**, a005181 (2011).
2. Munro, S. The golgin coiled-coil proteins of the Golgi apparatus. *Cold Spring Harb. Perspect. Biol.* **3**, a005256 (2011).
3. Lowe, M. The physiological functions of the golgin vesicle tethering proteins. *Front. Cell Dev. Biol.* **7**, 94 (2019).
4. Witkos, T. M. & Lowe, M. The golgin family of coiled-coil tethering proteins. *Front Cell Dev. Biol.* **3**, 86 (2015).
5. Panic, B., Perisic, O., Veprintsev, D. B., Williams, R. L. & Munro, S. Structural basis for Arl1-dependent targeting of homodimeric GRIP domains to the Golgi apparatus. *Mol. Cell* **12**, 863–874 (2003).
6. Barr, F. A. & Short, B. Golgins in the structure and dynamics of the Golgi apparatus. *Curr. Opin. Cell Biol.* **15**, 405–413 (2003).
7. Lu, L. & Hong, W. Interaction of Arl1–GTP with GRIP domains recruits autoantigens golgin-97 and golgin-245/p230 onto the Golgi. *Mol. Biol. Cell* **14**, 3767–3781 (2003).
8. Yu, C. J. & Lee, F. J. Multiple activities of Arl1 GTPase in the *trans*-Golgi network. *J. Cell Sci.* **130**, 1691–1699 (2017).
9. Tsai, P. C., Hsu, J. W., Liu, Y. W., Chen, K. Y. & Lee, F. J. Arl1p regulates spatial membrane organization at the *trans*-Golgi network through interaction with Arf-GEF Gea2p and flippase Drs2p. *Proc. Natl Acad. Sci. USA* **110**, E668–E677 (2013).
10. Chen, K. Y. et al. Syt1p promotes activation of Arl1p at the late Golgi to recruit Imh1p. *J. Cell Sci.* **123**, 3478–3489 (2010).
11. Sztul, E. et al. Arf GTPases and their GEFs and GAPs: concepts and challenges. *Mol. Biol. Cell* **30**, 1249–1271 (2019).
12. Chen, K. Y., Tsai, P. C., Liu, Y. W. & Lee, F. J. Competition between the golgin Imh1p and the GAP Gcs1p stabilizes activated Arl1p at the late-Golgi. *J. Cell Sci.* **125**, 4586–4596 (2012).
13. Wang, Y.-H. et al. Golgin Imh1 and GARP complex cooperate to restore the impaired SNARE recycling transport induced by ER stress. *Cell Rep.* **38**, 110488 (2022).
14. Hsu, J. W. et al. Unfolded protein response regulates yeast small GTPase Arl1p activation at late Golgi via phosphorylation of Arf GEF Syt1p. *Proc. Natl Acad. Sci. USA* **113**, E1683–E1690 (2016).
15. Tsai, H. J. et al. Hypo-osmotic-like stress underlies general cellular defects of aneuploidy. *Nature* **570**, 117–121 (2019).
16. Blomberg, A. Yeast osmoregulation—glycerol still in pole position. *FEMS Yeast Res.* **22**, foac035 (2022).
17. Levin, D. E. Cell wall integrity signaling in *Saccharomyces cerevisiae*. *Microbiol Mol. Biol. Rev.* **69**, 262–291 (2005).
18. Hohmann, S. Osmotic stress signaling and osmoadaptation in yeasts. *Microbiol Mol. Biol. Rev.* **66**, 300–372 (2002).
19. Vagenende, V., Yap, M. G. & Trout, B. L. Mechanisms of protein stabilization and prevention of protein aggregation by glycerol. *Biochemistry* **48**, 11084–11096 (2009).
20. Gekko, K. & Timasheff, S. N. Mechanism of protein stabilization by glycerol: preferential hydration in glycerol–water mixtures. *Biochemistry* **20**, 4667–4676 (1981).
21. Bolen, D. W. & Baskakov, I. V. The osmophobic effect: natural selection of a thermodynamic force in protein folding. *J. Mol. Biol.* **310**, 955–963 (2001).
22. Gekko, K. & Timasheff, S. N. Thermodynamic and kinetic examination of protein stabilization by glycerol. *Biochemistry* **20**, 4677–4686 (1981).
23. Sato, S., Ward, C. L., Krouse, M. E., Wine, J. J. & Kopito, R. R. Glycerol reverses the misfolding phenotype of the most common cystic fibrosis mutation. *J. Biol. Chem.* **271**, 635–638 (1996).
24. Bradbury, S. L. & Jakoby, W. B. Glycerol as an enzyme-stabilizing agent: effects on aldehyde dehydrogenase. *Proc. Natl Acad. Sci. USA* **69**, 2373–2376 (1972).
25. Corrêa, F. & Farah, C. S. Different effects of trifluoroethanol and glycerol on the stability of tropomyosin helices and the head-to-tail complex. *Biophys. J.* **92**, 2463–2475 (2007).
26. Klein, M., Swinnen, S., Thevelein, J. M. & Nevoigt, E. Glycerol metabolism and transport in yeast and fungi: established knowledge and ambiguities. *Environ. Microbiol.* **19**, 878–893 (2017).
27. Ram, A. F. et al. Loss of the plasma membrane-bound protein Gas1p in *Saccharomyces cerevisiae* results in the release of β1,3-glucan into the medium and induces a compensation mechanism to ensure cell wall integrity. *J. Bacteriol.* **180**, 1418–1424 (1998).
28. Futagami, T. et al. Putative stress sensors WscA and WscB are involved in hypo-osmotic and acidic pH stress tolerance in *Aspergillus nidulans*. *Eukaryot. Cell* **10**, 1504–1515 (2011).

29. Petelenz-Kurdziel, E. et al. Quantitative analysis of glycerol accumulation, glycolysis and growth under hyper osmotic stress. *PLoS Comput. Biol.* **9**, e1003084 (2013).

30. Cronwright, G. R., Rohwer, J. M. & Prior, B. A. Metabolic control analysis of glycerol synthesis in *Saccharomyces cerevisiae*. *Appl. Environ. Microbiol.* **68**, 4448–4456 (2002).

31. Toh, T.-H. et al. Implications of FPS1 deletion and membrane ergosterol content for glycerol efflux from *Saccharomyces cerevisiae*. *FEMS Yeast Res.* **1**, 205–211 (2001).

32. Lee, Y. J., Jeschke, G. R., Roelants, F. M., Thorner, J. & Turk, B. E. Reciprocal phosphorylation of yeast glycerol-3-phosphate dehydrogenases in adaptation to distinct types of stress. *Mol. Cell. Biol.* **32**, 4705–4717 (2012).

33. Pallapati, A. R., Sirigiri, S. D., Jain, S., Ratnala, V. & Roy, I. Lysine245 plays a crucial role in stability and function of glycerol 3-phosphate dehydrogenase (Gpd1) in *Saccharomyces cerevisiae*. *J. Cell. Biochem.* **122**, 1726–1736 (2021).

34. Gillingham, A. K., Tong, A. H., Boone, C. & Munro, S. The GTPase Arf1p and the ER to Golgi cargo receptor Erv14p cooperate to recruit the golgin Rud3p to the *cis*-Golgi. *J. Cell Sci.* **167**, 281–292 (2004).

35. Siniossoglou, S. & Pelham, H. R. An effector of Ypt6p binds the SNARE Tlg1p and mediates selective fusion of vesicles with late Golgi membranes. *EMBO J.* **20**, 5991–5998 (2001).

36. Hsu, J. W., Chen, Z. J., Liu, Y. W. & Lee, F. J. Mechanism of action of the flippase Drs2p in modulating GTP hydrolysis of Arl1p. *J. Cell Sci.* **127**, 2615–2620 (2014).

37. Setty, S. R., Shin, M. E., Yoshino, A., Marks, M. S. & Burd, C. G. Golgi recruitment of GRIP domain proteins by Arf-like GTPase 1 is regulated by Arf-like GTPase 3. *Curr. Biol.* **13**, 401–404 (2003).

38. Chen, S. et al. Roles for the Drs2p–Cdc50p complex in protein transport and phosphatidylserine asymmetry of the yeast plasma membrane. *Traffic* **7**, 1503–1517 (2006).

39. Kato, U. et al. A novel membrane protein, Ros3p, is required for phospholipid translocation across the plasma membrane in *Saccharomyces cerevisiae*. *J. Biol. Chem.* **277**, 37855–37862 (2002).

40. Sorger, D. & Daum, G. Triacylglycerol biosynthesis in yeast. *Appl. Microbiol. Biotechnol.* **61**, 289–299 (2003).

41. Sabir, F., Loureiro-Dias, M. C., Soveral, G. & Prista, C. Functional relevance of water and glycerol channels in *Saccharomyces cerevisiae*. *FEMS Microbiol. Lett.* **364**, fnx080 (2017).

42. Ferreira, C. & Lucas, C. Glucose repression over *Saccharomyces cerevisiae* glycerol/H$^+$ symporter gene *STL1* is overcome by high temperature. *FEBS Lett.* **581**, 1923–1927 (2007).

43. Ferea, T. L., Botstein, D., Brown, P. O. & Rosenzweig, R. F. Systematic changes in gene expression patterns following adaptive evolution in yeast. *Proc. Natl Acad. Sci. USA* **96**, 9721–9726 (1999).

44. Wu, M., Lu, L., Hong, W. & Song, H. Structural basis for recruitment of GRIP domain golgin-245 by small GTPase Arl1. *Nat. Struct. Mol. Biol.* **11**, 86–94 (2004).

45. Merzlyak, E. M. et al. Bright monomeric red fluorescent protein with an extended fluorescence lifetime. *Nat. Methods* **4**, 555–557 (2007).

46. Shearer, A. G. & Hampton, R. Y. Structural control of endoplasmic reticulum-associated degradation: effect of chemical chaperones on 3-hydroxy-3-methylglutaryl-CoA reductase. *J. Biol. Chem.* **279**, 188–196 (2004).

47. Fridmann-Sirkis, Y., Kent, H. M., Lewis, M. J., Evans, P. R. & Pelham, H. R. Structural analysis of the interaction between the SNARE Tlg1 and Vps51. *Traffic* **7**, 182–190 (2006).

48. Möller, M. & Denicola, A. Protein tryptophan accessibility studied by fluorescence quenching. *Biochem. Mol. Biol. Educ.* **30**, 175–178 (2002).

49. Ghosh, R., Roy, S. & Bagchi, B. Solvent sensitivity of protein unfolding: dynamical study of chicken villin headpiece subdomain in water–ethanol binary mixture. *J. Phys. Chem. B* **117**, 15625–15638 (2013).

50. Halder, R. & Jana, B. Exploring the role of hydrophilic amino acids in unfolding of protein in aqueous ethanol solution. *Proteins* **89**, 116–125 (2021).

51. Timasheff, S. N. Protein hydration, thermodynamic binding, and preferential hydration. *Biochemistry* **41**, 13473–13482 (2002).

52. Hirai, M. et al. Direct evidence for the effect of glycerol on protein hydration and thermal structural transition. *Biophys. J.* **115**, 313–327 (2018).

53. Baird, G. S., Zacharias, D. A. & Tsien, R. Y. Biochemistry, mutagenesis, and oligomerization of DsRed, a red fluorescent protein from coral. *Proc. Natl Acad. Sci. USA* **97**, 11984–11989 (2000).

Methods

Strains, plasmids, media and microbiological techniques

Supplementary Table 2 lists the yeast strains used in this study. Yeast cell culture conditions and medium preparation were preformed according to the descriptions in a previous study[54]. YP medium contained 1% Bacto yeast extract and 2% Bacto peptone. YPD medium contained 1% Bacto yeast extract, 2% Bacto peptone and 2% glucose. YPG medium is YP medium with 0.1 M glycerol. Synthetic defined medium contained 0.17% Difco yeast nitrogen base (without amino acids and ammonium sulfate), 0.5% ammonium sulfate and 2% glucose. Nutrients essential for auxotrophic strains were supplied at the specified concentrations. The lithium acetate method was used for yeast transformation[55] and gene disruption in yeast was based on a previously described protocol[54]. Supplementary Table 3 lists the plasmids used in this study. Plasmids were prepared according to a previously described protocol[56].

Antibodies

For western blotting, the following antibodies were used: anti-Imh1 (1:3,000), anti-PGP (1:1,000; A305-669A-M, Bethyl), and goat horseradish-peroxidase-conjugated anti-rabbit/mouse IgG (1:5,000; AP132P/AP124P, Millipore). For Immunofluorescence staining in mammalian cells, primary antibodies anti-B4GALT1 (1:200; ab121326, Abcam) and anti-p230 (1:100; 611281, BD) and secondary antibodies Alexa Fluor 488/594 goat anti-rabbit and anti-mouse IgG (1:1,000; A-11034/A-11012 and A-11001/A-11032, Invitrogen) were used. Rabbit polyclonal antibodies to Imh1 were produced in our previous studies[13,57].

Microscopy and fluorescence image analysis

Images of live cells carrying fluorescent fusion proteins were obtained after overnight culture in synthetic medium with 2% (w/v) glucose. Midlog-phase cells were observed and images were captured using a Zeiss Axioplan microscope equipped with a Cool Snap FX-camera (Carl Zeiss) using AxioVision Rel 4.8 software. For all microscopy examinations, the exposure times and image-processing procedures were identical for each sample within an experiment. The image experiments were analyzed using ImageJ Fiji software[58]. For quantification of colocalization between mCH (mCherry) or mRFP and GFP, channels were determined by ImageJ (version 1.51j8) Fiji software[59] with the Just Another Colocalization plugin and Costes automatic thresholding[60].

Hypo-osmotic shock treatment

WT yeast cells were transformed with mCH–Imh1 and Sec7–GFP and cultured in YPD medium for 12 h. The cells were then reinoculated in fresh YPD medium when the optical density at 600 nm (OD_{600}) was initially 0.2 and cultured for 2 h. For the double-distilled (dd)H_2O-induced hypo-osmotic shock, cells were grown in YPD, pelleted by centrifugation at 800g at room temperature for 3 min, suspended in ddH_2O for 5 min, pelleted by centrifugation and resuspended in YPD medium.

Glycerol rescue procedures for visualization

Cells transformed with mCH–Imh1 were cultured in YPD medium for 12 h. The cells were then reinoculated in fresh YPD medium when the OD_{600} was initially 0.2 and cultured for 2 h. Next, the cells were pelleted by centrifugation at 800g for 3 min and suspended in YPG medium for another 10 min of culture.

For the observation of Snc1 localization after TM (654380, Sigma) treatment, cells were transformed with GFP–Snc1 and cultured in YPD medium for 14 h. The cells were then reinoculated in fresh YPD medium with an initial OD_{600} of 0.2 and cultured for 2 h. After refreshing the cells, the cell culture medium was replaced with YPG medium for subsequent treatment with 1 µg ml^{-1} TM for 1.5 h and visualization.

Drug sensitivity assay

For a cinnamycin sensitivity assay, different yeast strains were cultured in YPD medium for 14 h. The cells were then reinoculated into fresh YPD medium with or without 30 µM cinnamycin (20136, Cayman) when the initial OD_{600} was 0.15 and cultured for 6 h. The drug sensitivity was determined by measuring the OD_{600} of the cultures every 2 h. The growth percentage was determined by dividing the increase in the OD_{600} value of the treated cells by that of the untreated cells.

Protein interaction analysis

To analyze the self-interaction of Imh1 in WT and $gpd1\Delta$ cells, cells were exogenously transformed with HA–Imh1 and Myc–Imh1. Cells were cultured in synthetic medium containing 2% glucose. After an overnight culture to midlog phase, yeast cells (100 OD_{600} units) were harvested and washed with 1 ml of 20 mM NaN$_3$, lysed with glass beads in 500 µl of lysis buffer (50 mM Tris-Cl pH 7.5, 100 mM NaCl, 10 mM MgCl$_2$, 1 mM EDTA pH 8.5, 0.1% NP-40 and a protease inhibitor) using glass beads beating for 8 min at 4 °C. After centrifugation at 800g at 4 °C for 5 min, the supernatants were collected and kept on ice and the remaining pellets were suspended in 500 µl of lysis buffer using glass beads beating for 8 min at 4 °C. All supernatants were combined and centrifuged at 3,500g for 10 min to collect clear cell lysate. The clarified cell lysate was then incubated with prewashed Myc-trap magnetic agarose (Chromotek, ytma-20) on an end-over-end rotator for 2 h at 4 °C and washed three times with lysis buffer. The bound proteins were then analyzed by western blot for the presence of HA–Imh1.

Purification of Imh1–His from yeast

For Imh1–His purification from yeast cells, $imh1\Delta$ and $gpd1imh1\Delta$ cells expressing Imh1–His grown in 200 ml of synthetic dropout medium with 2% (w/v) glucose to the midexponential phase ($OD_{600} = 0.5$) were harvested by centrifugation. Cells expressing Imh1–His cultured in 100 ml of synthetic medium with 2% (w/v) glucose to the midexponential phase ($OD_{600} = 1$) were harvested by centrifugation. Approximately 180 OD_{600} cells were washed with 20 mM NaN$_3$ and then incubated with a Zymolyase-100T mixture (5 mg ml^{-1} Zymolyase-100T and 1% β-mercaptoethanol) in potassium phosphate buffer (190 mM K$_2$HPO$_4$, 310 mM KH$_2$PO$_4$ and 1.2 M sorbitol in ddH_2O) at 30 °C for 1 h to form spheroplasts. The spheroplasts were washed three times with 1 ml of potassium phosphate buffer. The cell pellet was then suspended in 500 µl of cold lysis buffer (20 mM HEPES pH 6.8, 1 mM EDTA, 0.1 M sorbitol and 50 mM potassium phosphate) containing 1× protease inhibitors[13] in ddH_2O and disrupted by glass bead beating for 8 min. After the cell lysates were centrifuged at 800g at 4 °C for 5 min, the supernatants were collected and maintained on ice and the pellets were suspended in 500 µl of lysis buffer using glass bead beating for 8 min at 4 °C. All supernatants were combined and centrifuged at 3,500g for 5 min twice to collect clear cell lysates. The clarified cell lysates were then incubated with prewashed His-Pur Ni-NTA resin (Thermo Fisher Scientific, 88222) on an end-over-end rotator at 4 °C for 14 h and then washed twice with lysis buffer and an additional two times with wash buffer (20 mM Tris pH 8.0, 500 mM NaCl, 20 mM imidazole and 1× protease inhibitors). The bound Imh1–His on resin was eluted in 600 µl of elution buffer (20 mM Tris pH 8.0, 500 mM NaCl, 500 mM imidazole and 1× protease inhibitors) for 30 min.

Purification of His–Imh1-C213 from Escherichia coli

His–Imh1-C213 fragment (C-terminal 699–911 residues) was expressed in E. coli BL21 competent cells and induced at $OD_{595} = 0.6$–0.8 with 0.5 mM IPTG for 16 h at 16 °C. Then, the cells were lysed with lysis buffer (50 mM Na$_2$HPO$_4$, 300 mM NaCl, 20 mM imidazole, 0.1% Triton X-100, 10% glycerol and a 1× protease inhibitor cocktail) and treated with 1 mg ml^{-1} lysozyme for 30 min on ice. The lysates were then applied to a nitrogen bomb and centrifuged at 13,200g at 4 °C for 5 min and then the supernatants were incubated with His-Pur Ni-NTA resin (Thermo Fisher Scientific, 88222) for 2 h. After the Ni-NTA resin was washed three times with wash buffer (50 mM Na$_2$HPO$_4$, 300 mM NaCl, 50 mM imidazole and 1× protease inhibitor cocktail), the bound

His–Imh1-C213 on the resin was eluted with elution buffer (PBS with 250 mM imidazole) for 30 min.

Gel filtration analysis of Imh1 oligomerization

Purified His–Imh1-C213 from *E. coli* was dialyzed in PBS with or without 0.1 M glycerol for 14 h in a cold room. Then, 2 mg of His–Imh1-C213 from *E. coli* or 600 µl of purified Imh1–His from yeast cells was loaded onto a HiLoad 16/600 Superdex 200 pg column (Cytiva) with an AKTA pure system (Cytiva) and UNICORN 7.3 software (Cytiva), which was pre-equilibrated with PBS. Protein was eluted in PBS with or without glycerol. Absorbance was monitored at 280 nm. Protein in the fractions was mixed with 2× SDS sample buffer and then analyzed by western blotting.

Sedimentation velocity analysis by analytical ultracentrifugation

The sedimentation velocity experiment was conducted at the Institute of Biological Chemistry, Academia Sinica. The sample (OD_{280} = 0.2) in PBS was run at 20 °C and 307,450g in an XL-A analytical ultracentrifuge equipped with an ultraviolet–visible light absorbance detection system (Beckman-Coulter) and an an-60 Ti rotor. The sample was recorded by absorbance at 280 nm. The value of PBS density (1.00575 g ml^{-1}), viscosity (0.0010194 poise) and partial specific volume (0.73 ml g^{-1}) were calculated using SEDNTERP[61]. The sedimentation coefficient and molecular weight of Imh1-C213 were calculated from c(s) analysis using the continuous distribution c(s) Lamm equation model in SEDFIT[62].

SEC–MALS

His–Imh1-C213 was purified with His-Pur Ni-NTA resin, further purified over the Superdex 200 Increase 10/300 GL SEC column with an AKTA pure system (Cytiva) and then concentrated with Amicon. The SEC–MALS experiment was performed in the Biophysical Instrumentation Laboratory at the Institute of Biological Chemistry, Academia Sinica. The SEC–MALS measurements were performed using a miniDAWN TREOS detector (Wyatt Technology Corporation) coupled to an Agilent 1260 Infinity high-performance LC (HPLC) instrument. His–Imh1-C213 protein (100 µl) at a concentration of 2.27 mg ml^{-1} was injected into a Superdex 200 Increase 10/300 GL SEC column (Cytiva) and continuously run at a flow rate of 0.5 ml min^{-1} in PBS. Molecular weights were determined by MALS using an inline miniDAWN TREOS detector and an Optilab T-rEX differential refractive index detector (Wyatt Technology Corporation). BSA (A1900, Sigma) was used as the calibration standard and data were analyzed using ASTRA 6 software (Wyatt Technology Corporation) with the dn/dc value set to 0.185 ml g^{-1}.

Mass photometry

The mass photometry analysis was performed in the Biophysical Instrumentation Laboratory at the Institute of Biological Chemistry, Academia Sinica. His–Imh1-C213 (7.5 nM) was applied to a TwoMP mass photometer (Refeyn). The calibration curve was obtained from the measurements of BSA (monomers, 66 kDa; dimers, 132 kDa; trimer, 198 kDa) to determine the mass of His–Imh1-C213. The data were analyzed using Refeyn DiscoverMP software (Refeyn).

Limited proteolysis assay

Recombinant His-tagged Imh1-C213 fragment (C-terminal 699–911 residues) and the GST–Tlg1 (1–206) transmembrane domain truncation mutant were expressed and purified from *E. coli* as described previously[12]. Then, 5 µg of His-tagged recombinant protein was preincubated with or without 0.1 M glycerol in 20 mM Tris pH 8 and 100 mM NaCl buffer at 30 °C for 30 min before adding 5 mM (0.035%) β-mercaptoethanol at 30 °C for another 30 min (ref. 63). The treated proteins were then digested by trypsin (T8003, Sigma) (1:20 w/w ratio to protein) on ice for the time indicated. Reactions were halted by adding 2× sample buffer (100 mM Tris pH 6.8, 4% SDS, 0.2% bromophenol

blue, 20% glycerol and 4% β-mercaptoethanol) and boiled at 95 °C for 10 min. Imh1 and GST–Tlg1 (1–206) were resolved on 12% or 10% SDS–PAGE, respectively, and then stained with Coomassie brilliant blue.

Chemical crosslinking

Purified Imh1-C213 was exchanged for crosslinking buffer (10 mM HEPES pH 8.5 and 100 mM NaCl) by passing it through an SEC column Superdex 200 Increase 10/300 GL (Cytiva). The protein was then incubated with or without 0.1 M glycerol in crosslinking buffer at 30 °C for 1 h. Crosslinking was carried on by incubating 0.1 mg ml^{-1} Imh1-C213 with 0.1 mM d_0 or d_4 BS3 (21590/21595, Thermo Fisher Scientific) at 25 °C for 30 min. The crosslinking step was repeated with label swapping. The crosslinking reaction was finally quenched with 50 mM Tris and incubated at 25 °C for 15 min.

In-solution digestion

For protein digestion, equal amounts of BS3-labeled Imh1-C213 protein (d_0:d_4 = 1:1) were dissolved in a solution of 100 mM triethylammonium bicarbonate and subjected to reduction with 5 mM tris(2-carboxyethyl)phosphine and alkylation with 10 mM methyl methanethiosulfonate in the dark. Samples were digested with trypsin (Promega) at an enzyme-to-protein ratio of 1:25 at 37 °C overnight. Desalting was performed using a SOURCE 15RPC reversed-phase microcolumn (Cytiva) and the resulting peptide mixture was dried in a SpeedVac concentrator. The dried peptides were then resuspended in a 0.1% formic acid (FA; Sigma) solution for further MS analysis.

LC–MS/MS analysis

LC–MS/MS analysis was performed as previously described[64] with some modifications. In brief, the crosslinked peptide mixtures in HPLC buffer (0.1% FA) were loaded onto a trap column (Zorbax 300SB-C18 column, 5 µm, 300 Å, 0.3 × 5 mm; Agilent Technologies) at a flow rate of 0.3 µl min^{-1}. The salts were washed with HPLC buffer at a flow rate of 20 µl min^{-1} for 10 min and the desalted peptides were then separated on a 10-cm analytical C18 column (Acquity UPLC M-Class Peptide BEH C18 column, 130 Å, 1.7 µm, 100 µm × 100 mm; Waters) using a 150-min linear gradient of 99.9% acetonitrile and 0.1% FA. The LC setup was coupled online to an LTQ-Orbitrap Elite Hybrid MS instrument (Thermo Fisher Scientific) operated with Xcalibur 2.2 software (Thermo Fisher Scientific). The experimental apparatus was operated under conditions of positive ionization mode, with the applied spray voltage set to 1.8 kV. Acquisition of MS1 spectra in an MS range of 400–2,000 Da (m/z 400–800, 700–1,100 and 1,000–1,400) was performed using the Orbitrap mass analyzer. For MS2, a higher-energy collisional dissociation with a normalized collision energy of 30% was set for the fragmentation. The resolution was set to 120,000 and 15,000 for MS1 and MS2, respectively. The dynamic exclusion was set to 60 s and the top ten ions with the highest intensity were selected for fragmentation. For data analysis, raw spectral data were uploaded to the pLink3 search engine[65] (version 3.0.16, released on 11 January 2025) to identify and quantify crosslinks. A FASTA database for the Imh1-C213 sequence was created on the basis of UniProt. The parameters for the pLink3 search included BS3 and BS3 heavy as crosslinkers, with trypsin as the protease, allowing for a maximum of two missed cleavages. Methylthiocysteine was designated as a fixed modification, while oxidation of methionine was treated as a variable modification. Mass tolerances were set at 10 ppm for MS1 and 20 ppm for MS2 data. A false discovery rate of 1% at the spectrum level was applied[66]. Only crosslinked peptide pairs with BS3 linkages at lysine residues were included in the analysis, while crosslinks at peptide C termini were excluded, except for those involving the C terminus of the Imh1-C213 protein. Annotated *b* and *y* ions corresponding to the peptide sequences were generated from the identified crosslinks and visualized using pLabel software (version 2.4.3). To ensure robustness, a quantitative analysis was performed using a triplicate label-swap approach. Crosslinks considered for

quantification in six independent experiments were those that had at least one crosslinked peptide spectrum match with a pLink3 spectrum score greater than 0.85 in each experiment and the spectrum quality was manually verified.

Intrinsic tryptophan fluorescence

Intrinsic tryptophan fluorescence measurements were performed using an Infinite M1000 PRO microplate reader (Tecan). His–Imh1-C213 was first incubated with or without 0.1 M glycerol at 37 °C for 1 h in PBS. Samples (10 μM) were loaded in duplicates (2 × 100 μl) in a 96-well polypropylene F-bottom plate (Greiner Bio-One International). Emission spectra were recorded from 300 to 450 nm with an increment of 1 nm (bandwidth: 10 nm) using an excitation wavelength of 280 nm (bandwidth: 10 nm). The measurements were conducted with a gain of 90, a Z position of 19,000 μm and 30 light flashes per single measurement. Data were processed using Excel.

Cell culture

The human epithelial cell line HeLa (CCL-2) was from the American Type Culture Collection and cells were grown in DMEM high glucose (Cytiva, SH30003.02) with 10% FBS (Gibco, 10437-028) in a humidified incubator with 5% CO_2 at 37 °C. The cell line was authenticated using short tandem repeat analysis. Fluorescent DNA staining using Hoechst 33258 confirmed the cell cultures to be *Mycoplasma*-free.

Immunofluorescence staining in mammalian cells

HeLa cells (CCL-2) were seeded on 12-mm microscope coverslips (Assistant) and treated with siRNA against PGP (Dharmacon, J-022877-06-0005 (siPGP6) and J-022877-07-0005 (siPGP7)) using RNAiMAX (56532, Invitrogen) transfection reagent according to the manufacturer's protocol for 48 h. The indicated groups were supplied with 0.1 M glycerol (A3707.1000, PanReac Applichem) in the medium for an additional hour. Cells were washed immediately and fixed with 4% paraformaldehyde before immunofluorescence staining as previously described[64]. Notably, primary antibodies were stained at 4 °C overnight. Cell images were captured with a ×40 oil immersion objective lens with an Axioplan 2 microscope (Carl Zeiss). The images, obtained after conversion into IMS files by ImarisFileConverter 9.9.1, were analyzed using Imaris 9.8.0 software with the 'surface' module for determining the 'number of disconnected components per time point' to measure the number of nuclei and Golgi protein fragments in different color channels. The 'smooth' function was selected. 'Background subtraction (local contrast)' was used to define the targeting components. In Imaris software, the diameter for the nucleus was 14.5 μm, while it was 0.5 μm and 0.4 μm for the Golgi markers p230 and B4GALT1, respectively. All masks were applied consistently in all images obtained from the same biological batch. The number of fragments per cell was obtained by dividing the 'number of disconnected components (Golgi marker channel)' by the 'number of disconnected components (nuclear channel)' in a field.

Statistics and reproducibility

For panels with quantification results, N indicates the number of biological replicates and n indicates the sample size. All statistical data are displayed as the mean ± s.d. with three biological replicates. The statistical data were analyzed using GraphPad Prism 9.0 (GraphPad Software). Plots displaying layered data are shown as superplots[67]. To compare two groups, a two-sided unpaired Student's t-test was used. For analyses involving multiple groups or conditions, a one-way or two-way analysis of variance (ANOVA) was applied. A P value < 0.05 was considered statistically significant. No statistical methods were used to predetermine the sample size and no data were excluded from the analysis.

Reporting summary

Further information on research design is available in the Nature Portfolio Reporting Summary linked to this article.

Data availability

The MS data were deposited to the ProteomeXchange consortium through the PRIDE partner repository[68] with the dataset identifier PXD061125. The FASTA file of the Imh1-C213 sequence was derived from UniProt with accession code Q06704. All data generated or analyzed during this study are included in this published article and its Supplementary Information. All other data supporting the findings of this study are available from the corresponding authors on reasonable request. Source data are provided with this paper.

References

54. Liu, Y. W., Lee, S. W. & Lee, F. J. Arl1p is involved in transport of the GPI-anchored protein Gas1p from the late Golgi to the plasma membrane. *J. Cell Sci.* **119**, 3845–3855 (2006).
55. Ito, H., Fukuda, Y., Murata, K. & Kimura, A. Transformation of intact yeast cells treated with alkali cations. *J. Bacteriol.* **153**, 163–168 (1983).
56. Green, M. R. & Sambrook, J. *Molecular Cloning: A Laboratory Manual* 4th edn (Cold Spring Harbor Laboratory, 2012).
57. Chen, Y. T. et al. Action of Arl1 GTPase and golgin Imh1 in Ypt6-independent retrograde transport from endosomes to the *trans*-Golgi network. *Mol. Biol. Cell* **30**, 1008–1019 (2019).
58. Xu, P. et al. COPI mediates recycling of an exocytic SNARE by recognition of a ubiquitin sorting signal. *eLife* **6**, e28342 (2017).
59. Hankins, H. M., Sere, Y. Y., Diab, N. S., Menon, A. K. & Graham, T. R. Phosphatidylserine translocation at the yeast trans-Golgi network regulates protein sorting into exocytic vesicles. *Mol. Biol. Cell* **26**, 4674–4685 (2015).
60. Bolte, S. & Cordelières, F. P. A guided tour into subcellular colocalization analysis in light microscopy. *J. Microsc.* **224**, 213–232 (2006).
61. Laue, T. M., Shah, B., Ridgeway, T. M. & Pelletier, S. L. Computer-aided interpretation of sedimentation data for proteins. In *Analytical Ultracentrifugation in Biochemistry and Polymer Science* (eds Harding, S. E., Horton, J. C. & Rowe, A. J.) (Royal Society of Chemistry, 1992).
62. Schuck, P. Size-distribution analysis of macromolecules by sedimentation velocity ultracentrifugation and Lamm equation modeling. *Biophys. J.* **78**, 1606–1619 (2000).
63. Olsen, R. K. J. et al. Riboflavin-responsive and -non-responsive mutations in FAD synthase cause multiple acyl-CoA dehydrogenase and combined respiratory-chain deficiency. *Am. J. Hum. Genet.* **98**, 1130–1145 (2016).
64. Lin, M. C., Yu, C. J. & Lee, F. S. Phosphorylation of Arl4A/D promotes their binding by the HYPK chaperone for their stable recruitment to the plasma membrane. *Proc. Natl Acad. Sci. USA* **119**, e2207414119 (2022).
65. Chen, Z.-L. et al. A high-speed search engine pLink 2 with systematic evaluation for proteome-scale identification of cross-linked peptides. *Nat. Commun.* **10**, 3404 (2019).
66. Linden, A. et al. A cross-linking mass spectrometry approach defines protein interactions in yeast mitochondria. *Mol. Cell. Proteom.* **19**, 1161–1178 (2020).
67. Lord, S. J., Velle, K. B., Mullins, R. D. & Fritz-Laylin, L. K. SuperPlots: communicating reproducibility and variability in cell biology. *J. Cell Biol.* **219**, e202001064 (2020).
68. Griss, J. et al. Recognizing millions of consistently unidentified spectra across hundreds of shotgun proteomics datasets. *Nat. Methods* **13**, 651–656 (2016).
69. Abramson, J. et al. Accurate structure prediction of biomolecular interactions with AlphaFold 3. *Nature* **630**, 493–500 (2024).

Author contributions

W.-Y.C., C.-J.Y. and F.-J.S.L. designed the study and interpreted the results. W.-Y.C. performed most of the experiments and analyzed the presented data. Y.-H.W. and C.-C.L. contributed new reagents and assisted in the experiments. M.-C.L. performed experiments with mammalian cells. C.-J.Y. contributed reagents and tools for protein crosslinking mass analysis and interpreted the results. W.-Y.C., C.-J.Y. and F.-J.S.L. wrote the paper. C.-J.Y. and F.-S.J.L. supervised the project, acquired funding and performed project administration. All authors discussed the results and edited the paper.

Competing interests

The authors declare no competing interests.

Additional information

Extended data is available for this paper at https://doi.org/10.1038/s41594-025-01600-x.

Supplementary information The online version contains supplementary material available at https://doi.org/10.1038/s41594-025-01600-x.

Correspondence and requests for materials should be addressed to Chia-Jung Yu or Fang-Jen S. Lee.

Peer review information *Nature Structural & Molecular Biology* thanks Robert Ernst and the other, anonymous, reviewer(s) for their contribution to the peer review of this work. Peer reviewer reports are available. Primary Handling Editors: Carolina Perdigoto, Katarzyna Ciazynska and Melina Casadio, in collaboration with the *Nature Structural & Molecular Biology* team.

Reprints and permissions information is available at www.nature.com/reprints.
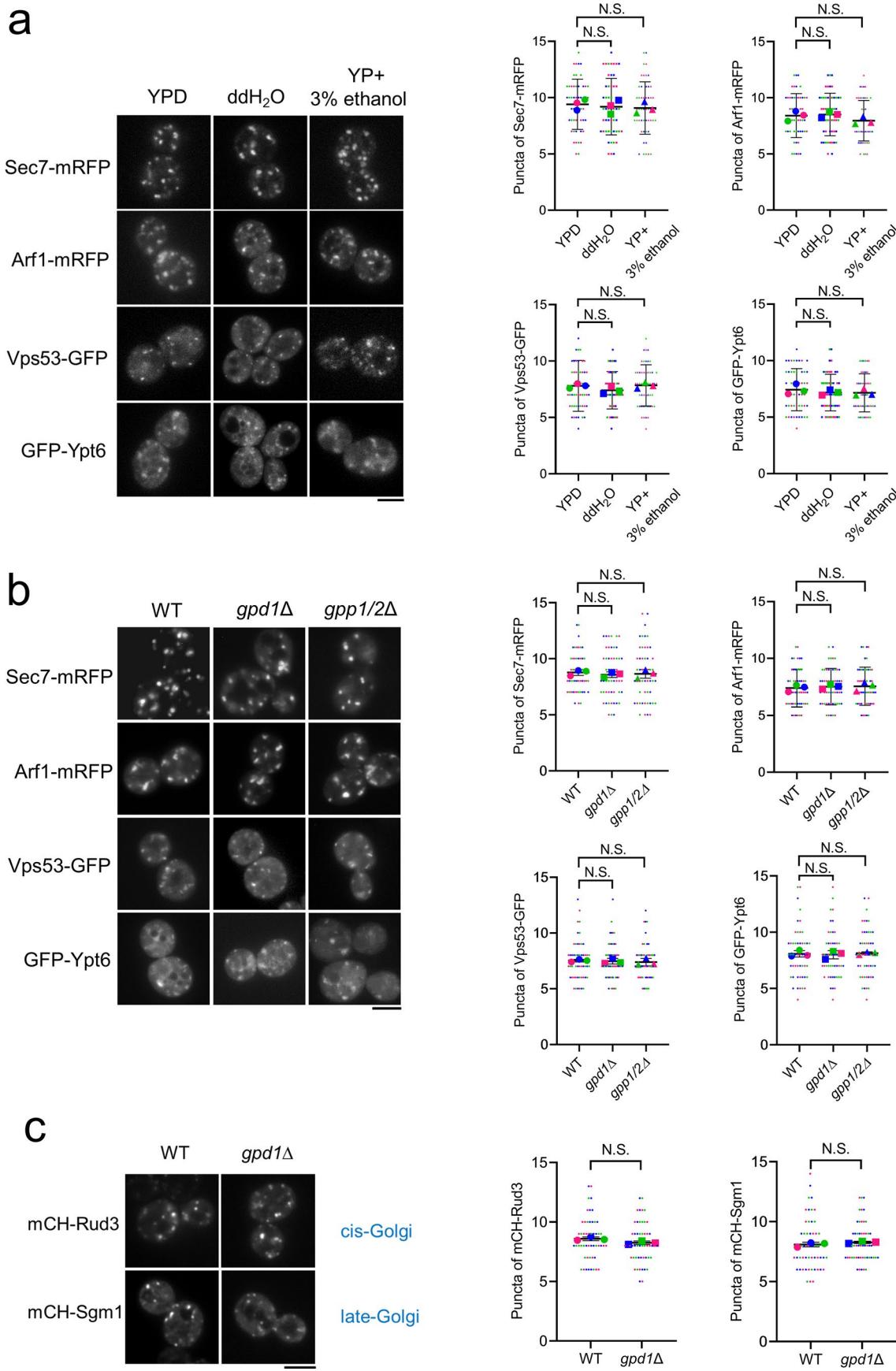
Extended Data Fig. 1 | See next page for caption.

Extended Data Fig. 1 | Golgi localization of various proteins is not affected under hypo-osmotic or ethanol treatment conditions and in glycerol-deficient cells. (**a**) Golgi-resident proteins are not affected under hypo-osmotic or ethanol treatment conditions. Sec7-mRFP (late-Golgi marker), Arf1-mRFP (Golgi marker), Vps53-GFP, or GFP-Ypt6 were expressed in WT cells. The live cells were cultured in YPD medium until mid-log phase. For hypo-osmotic shock treatment, the medium was removed, and the cells were suspended in water for 5 min. For ethanol treatment, the medium was removed and the cells were suspended in YP medium containing 3% ethanol for 10 min. Scale bar, 5 μm. (**b**) Golgi-resident proteins are not affected in glycerol-deficient cells. Sec7-mRFP (late-Golgi marker), Arf1-mRFP (Golgi marker), Vps53-GFP, or GFP-Ypt6 was expressed in WT, *gpd1Δ*, and *gpp1/2Δ* cells. (**c**) The localization of Golgin protein Rud3 and Sgm1 is not affected in glycerol-deficient cells. mCH-Rud3 or Sgm1 was expressed in WT and *gpd1Δ* cells. (**b-c**) Live cells were observed in mid-log phase. Scale bar, 5 μm. (**a-b**) The number of Sec7-mRFP, Arf1-mRFP, Vps53-GFP, and GFP-Ypt6 puncta was determined using ImageJ Fiji software (N = 3, n = 50). Data are presented as the mean ± SD of three independent experiments. (N.S., not significant; one-way ANOVA with Dunnett's post hoc multiple comparison test, no treatment or WT cells were used as reference) (**c**) The number of mCH-Rud3 and Sgm1 puncta was determined using ImageJ Fiji software (N = 3, n = 50). Data are presented as the mean ± SD of three independent experiments. (N.S., not significant; two-sided unpaired t test).
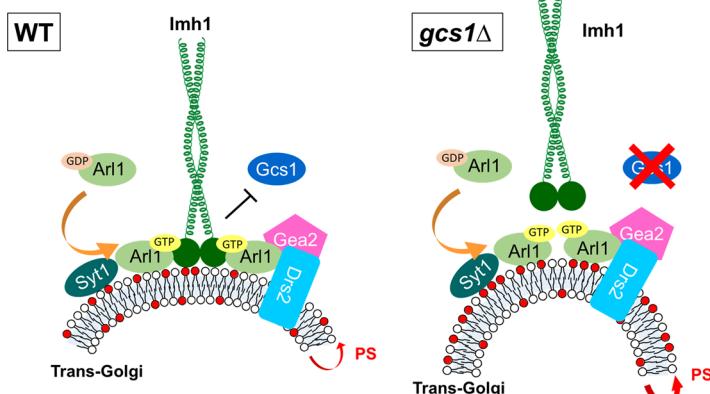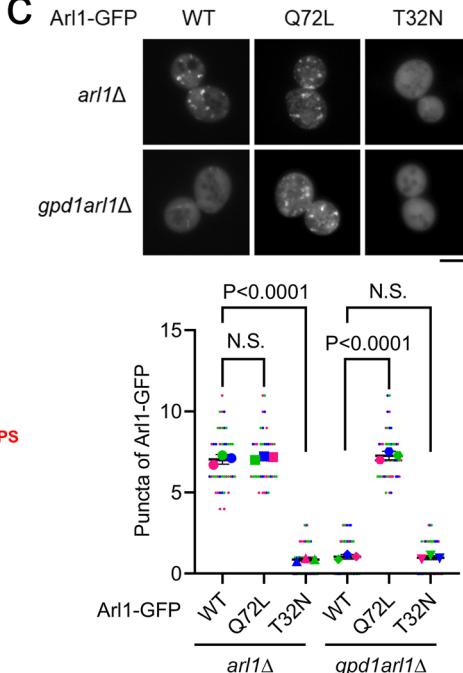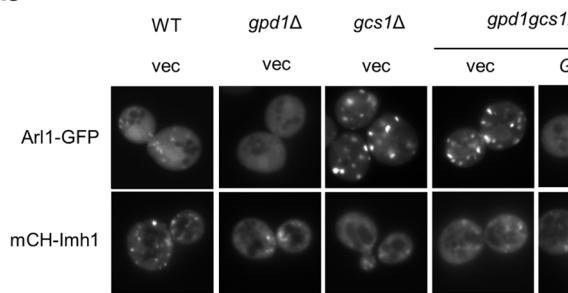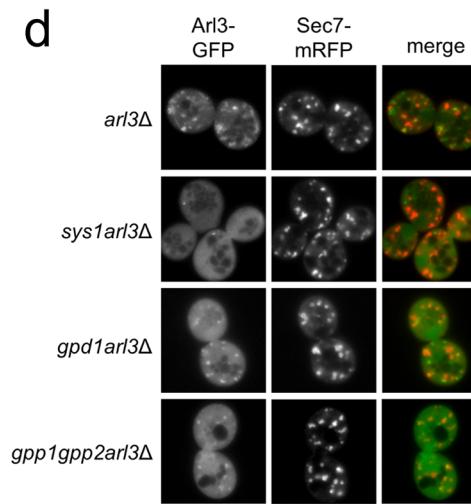
Extended Data Fig. 2 | See next page for caption.

Extended Data Fig. 2 | Gpd1 regulates the localization of Imh1. (a) Diagram of Imh1 stabilizing the Arl1-Imh1 complex by inhibiting Gcs1, which catalyzes GTP hydrolysis. Activated Arl1 recruits downstream Imh1 and forms a stable complex, which prevents Gcs1 from promoting GTP hydrolysis. PS, phosphatidylserine. (b) Arl1 localization is restored in *gpd1gcs1Δ* cells. Arl1-GFP or mCH-Imh1 was expressed in the indicated strains. Live cells were observed in mid-log phase. The number of mCH-Imh1 and Arl1-GFP puncta was determined using ImageJ Fiji software (N = 3, n = 50). Data are presented as the mean ± SD of three independent experiments. (N.S., not significant; one-way ANOVA with Dunnett's post hoc multiple comparison test, WT cells were used as reference) Scale bar, 5 μm. (c) Arl1^{Q72L}-GFP maintains Golgi localization in *gpd1Δ* cells. Arl1-GFP, Arl1^{Q72L}-GFP (constitutively active), or Arl1^{T32N}-GFP (constitutively inactive) was expressed in *arl1Δ* and *gpd1arl1Δ* cells.

Live cells were observed in mid-log phase. The number of Arl1-GFP puncta was determined using ImageJ Fiji software (N = 3, n = 50). Data are presented as the mean ± SD of three independent experiments. (N.S., not significant; one-way ANOVA with Dunnett's post hoc multiple comparison test, Arl1-GFP in *arl1Δ* or *gpd1arl1Δ* cells were used as reference) Scale bar, 5 μm. (d) The localization of Arl3 is not affected in glycerol-deficient cells. Arl3-GFP and Sec7-mRFP were co-expressed in the indicated cells. Live cells were observed in mid-log phase. The ratio of colocalization between Arl3 and Golgi marker Sec7 was quantified (N = 3, n = 50). PCC, Pearson's correlation coefficient. The data are presented as the mean ± SD of three independent experiments. (N.S., not significant; one-way ANOVA with Dunnett's post hoc multiple comparison test, WT strain was used as reference). Scale bar, 5 μm.
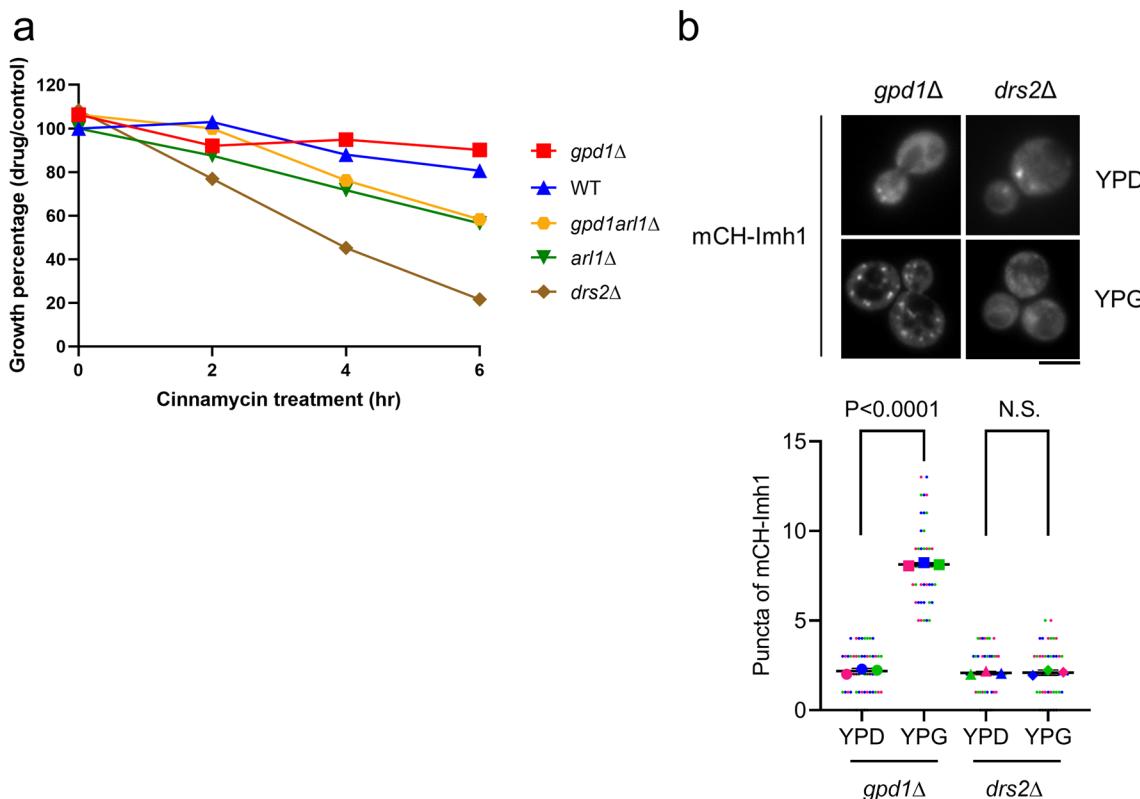
Extended Data Fig. 3 | Gpd1 deletion impairing Imh1 localization is not via affecting Drs2 activity. (**a**) *gpd1*Δ cells do not show sensitivity to cinnamycin. Cells were cultured to mid-log phase and treated with or without 30 µM cinnamycin for 6 h at 30 °C. The growth percentage every 1 h was determined by dividing the optical density of the treated strain obtained at 600 nm by that of the untreated control. (**b**) Glycerol fails to restore mislocalized Imh1 in *drs2*Δ cells. mCH-Imh1 was expressed in WT and *drs2*Δ cells. Cells were grown to mid-log phase in YPD medium and then transferred to YPG medium (YP medium containing 0.1 M glycerol) for 10 min. The number of mCH-Imh1 puncta was determined using ImageJ Fiji software (N = 3, n = 50). Data are presented as the mean ± SD of three independent experiments. (N.S., not significant; two-sided unpaired t test). Scale bar, 5 µm.
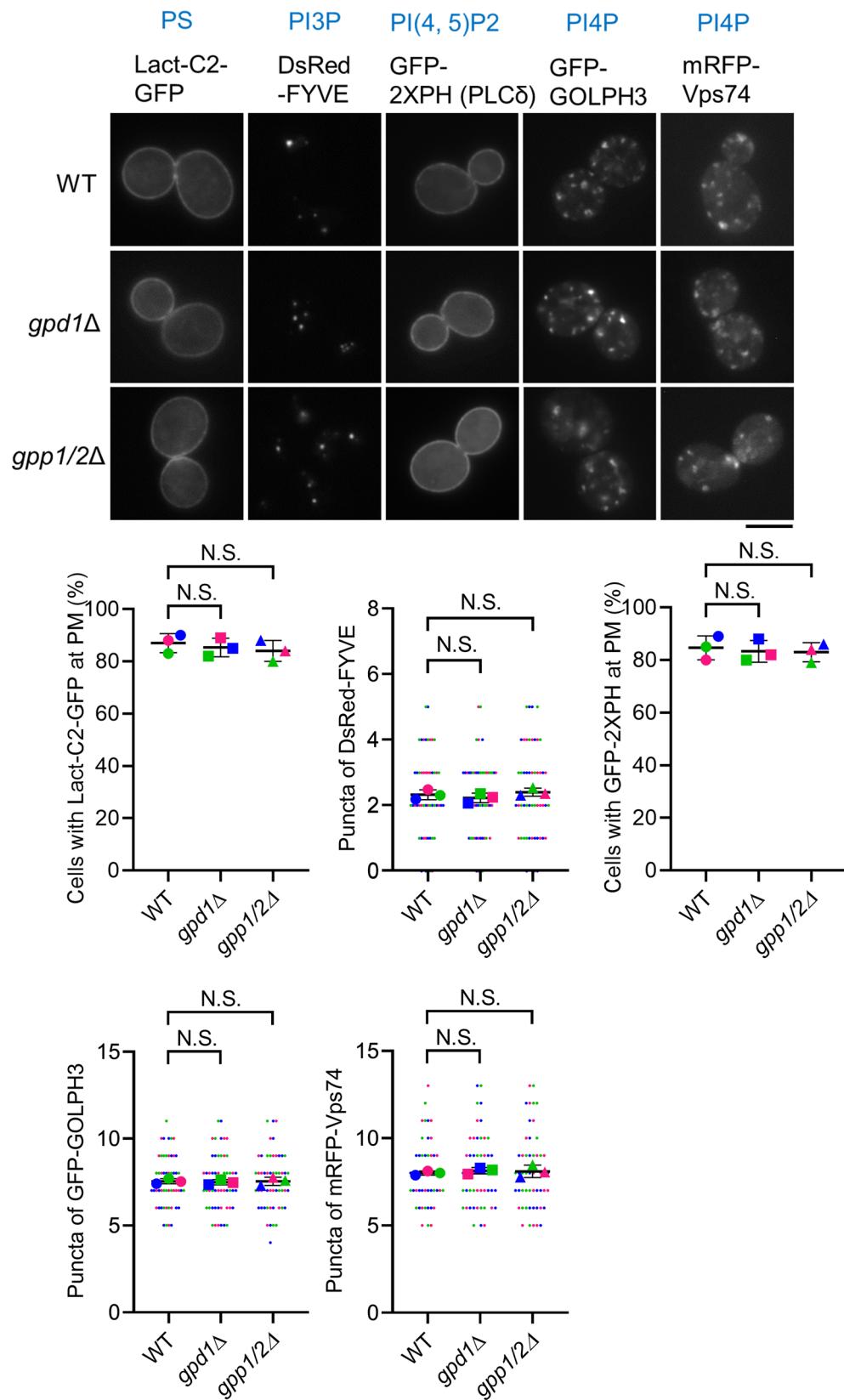
Extended Data Fig. 4 | Phospholipid-binding proteins are not affected in glycerol-deficient cells. Lactadherin-C2-GFP (lact-C2-GFP, phosphatidylserine-specific probe), DsRed-FYVE (phosphatidylinositol 3-phosphate probe), GFP-2xPH-PLCδ (phosphatidylinositol 4,5-bisphosphate-specific probe), GFP-GOLPH3 (phosphatidylinositol 4-phosphate probe), or mRFP-Vps74 (phosphatidylinositol 4-phosphate probe) was expressed in WT, *gpd1Δ*, and *gpp1/2Δ* cells. Live cells were observed in mid-log phase. The number of DsRed-FYVE, GFP-GOLPH3 and mRFP-Vps74 puncta was determined using ImageJ Fiji software (N = 3, n = 50). Cells showing the lact-C2-GFP or GFP-2xPH-PLCδ plasma membrane signal were quantified (N = 3, n = 50). The data are presented as mean ± SD of three independent experiments. (N.S., not significant; one-way ANOVA with Dunnett's post hoc multiple comparison test, WT strain was used as a reference). Scale bar, 5 μm.
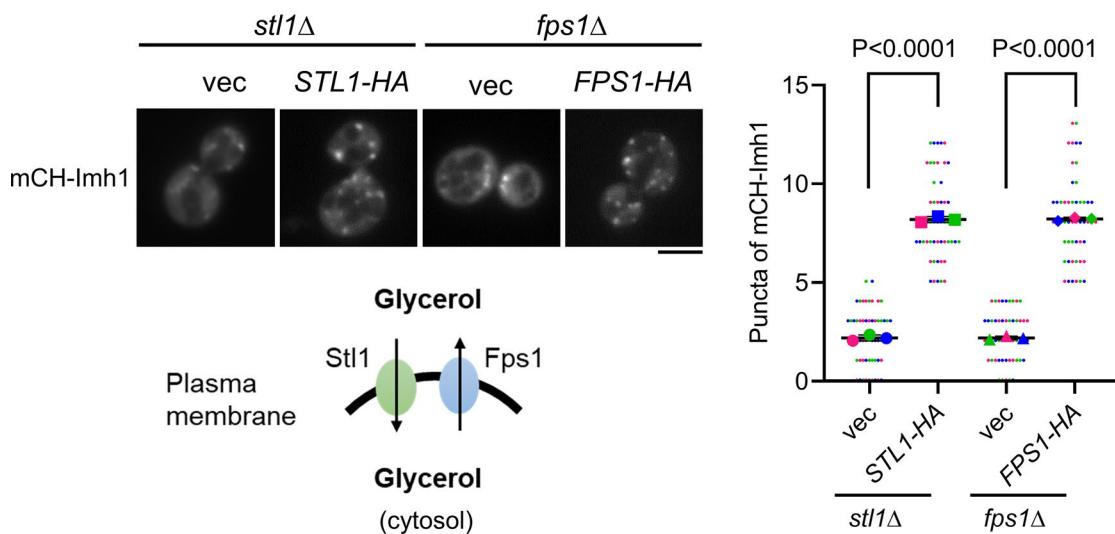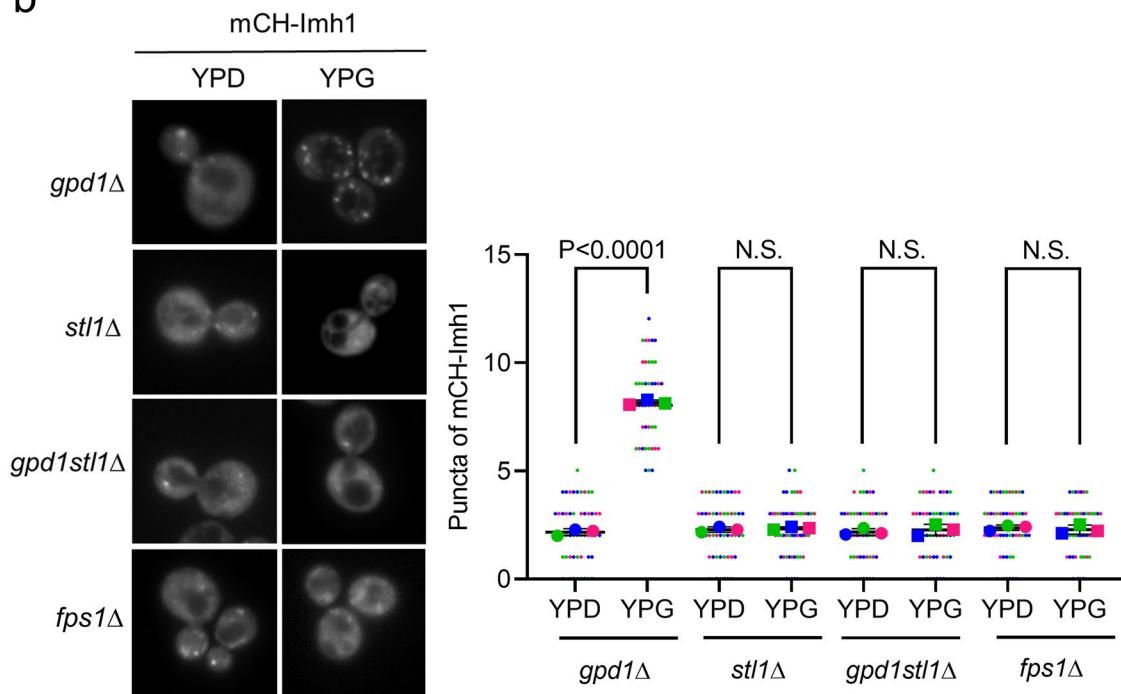
Extended Data Fig. 5 | Glycerol fails to restore the Imh1 localization in glycerol channel mutant cells. (**a**) Expression of Stl1 and Fps1 could rescue the localization of Imh1 in *stl1Δ*, and *fps1Δ* cells, respectively. Cells expressing with mCH-Imh1 was coexpressed with Stl1 or Fps1 in *stl1Δ* or *fps1Δ* cells, respectively. Live cells were observed in mid-log phase. (Scale bar, 5 μm.) Model depicts glycerol entry in yeast cells. (**b**) Glycerol fails to restore the localization of Imh1 in *stl1Δ* and *fps1Δ* cells. mCH-Imh1 was expressed in *gpd1Δ*, *fps1Δ*, *stl1Δ*, and *gpd1stl1Δ* cells. Cells were grown to mid-log phase in YPD, then medium was removed and cells were suspended in YP containing 0.1 M glycerol for 10 min. (Scale bar, 5 μm.) (**a-b**) The number of mCH-Imh1 puncta was determined using ImageJ Fiji software (N = 3, n = 50). Data are presented as the mean ± SD of three independent experiments. (N.S., not significant; two-sided unpaired t test).
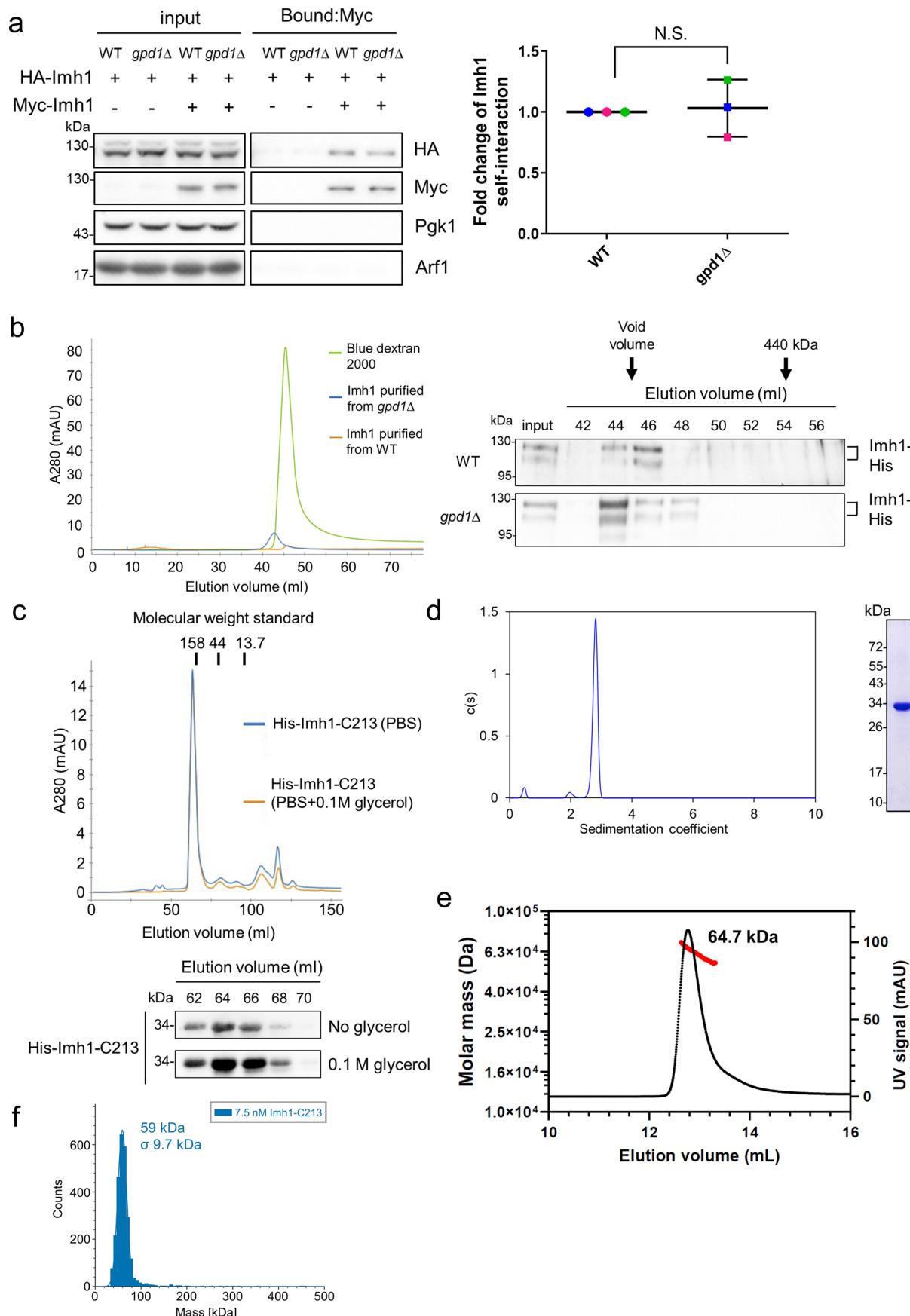
Extended Data Fig. 6 | See next page for caption.

**Extended Data Fig. 6 | Glycerol deficiency did not affect Imh1 oligomerization.**
(**a**) Imh1 self-interaction remained unaffected in *gpd1Δ* cells *in vivo*. Cells expressing HA-Imh1 and Myc-Imh1 were lysed, centrifuged to collect clear lysate, and incubated with Myc-Trap Magnetic Agarose. Bound proteins were analyzed by Western blotting, measuring intensities of bound HA-Imh1, bound Myc-Imh1, and input HA-Imh1 by ImageJ Fiji software. Bound HA-Imh1 signals were normalized to the bound Myc-Imh1 and input HA-Imh1 and the results for *gpd1Δ* cells were compared with those of WT cells. Data are reported as the mean ± SD of three independent experiments (N.S. not significant; two-sided unpaired t test). (**b**) Imh1-His was eluted with the oligomerized complex in yeast WT and *gpd1Δ* cells. Imh1-His was purified from WT and *gpd1Δ* cells eluted from HisPur Ni-NTA resin. (**c**) Glycerol does not affect the oligomerization of recombinant His-Imh1-C213 *in vitro*. His-Imh1-C213 was purified from *E. coli*, eluted from HisPur Ni-NTA resin, and dialyzed in PBS with or without 0.1 M glycerol overnight.

(**b**)(**c**) The protein was subjected to size exclusion chromatography on a HiLoad 16/600 Superdex 200 pg column in the indicated buffers. Fractions were analyzed via Western blot with an anti-Imh1 antibody. Blue dextran 2000 was used to determine the void volume. (**d**) Sedimentation velocity analysis of Imh1-C213 shows a sedimentation coefficient of 2.8, yielding a dimer peak with a molecular weight of 54.4 kDa. Purified recombinant Imh1-C213 in SDS-PAGE shows a single band at 34 kDa. (**b-d**) Each of the experiments was performed twice. (**e**) Size exclusion chromatography with multi-angle static light scattering (SEC-MALS) showed a calculated molar mass of approximately 64.7 kDa for the major peak of Imh1-C213, indicating a dimer. The black line shows UV at 280 nm, and the red line represents the molar mass measured with MALS. (**f**) Mass photometry analysis of Imh1-C213 showed a predominant peak at 59 kDa, representing the dimeric form of Imh1-C213.
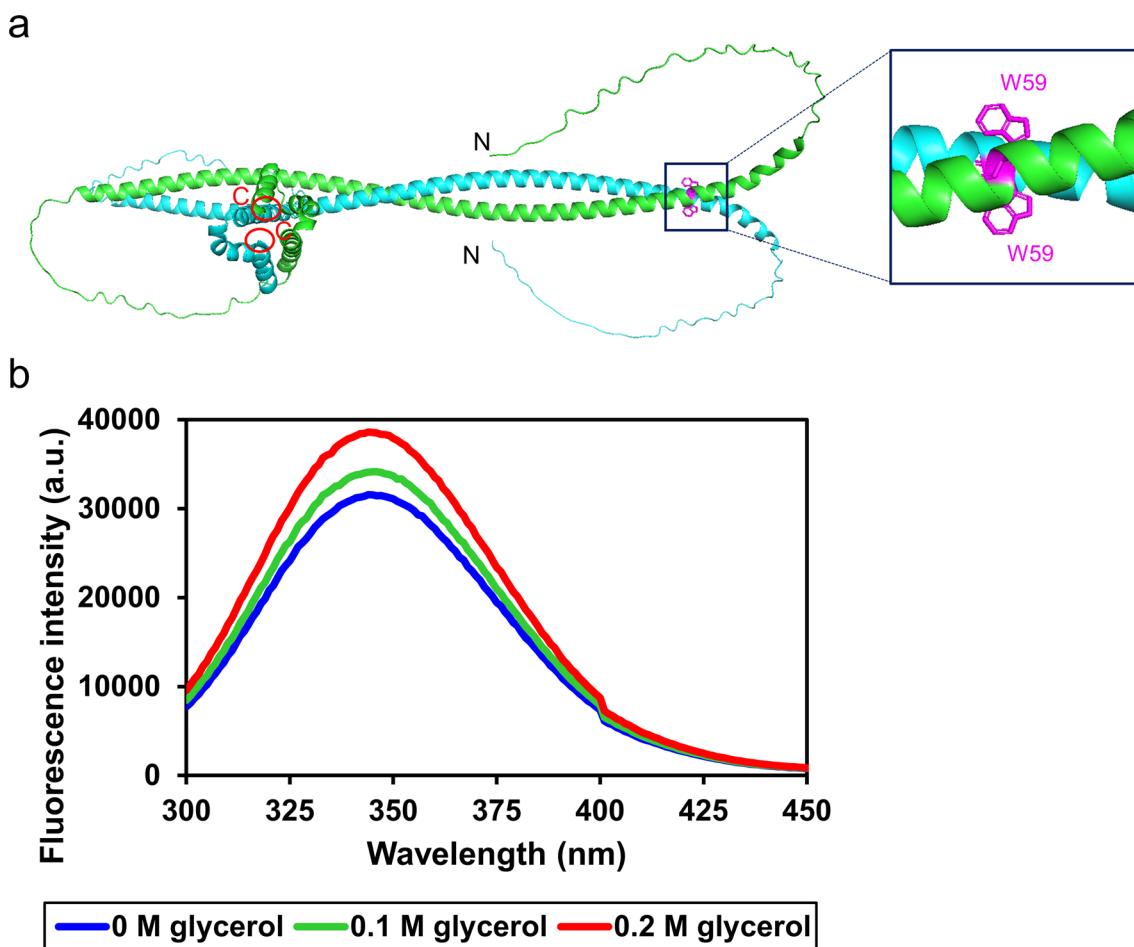
Extended Data Fig. 7 | Intrinsic tryptophan fluorescence of Imh1-C213 is affected in the presence of glycerol. (a) AlphaFold3 prediction model[69] of His-Imh1-C213 dimer. The tryptophan residue in the 59th residue (magenta W59) is shown as stick model. **(b)** Intrinsic tryptophan fluorescence emission spectra of Imh1-C213 after treatment with 0.1 or 0.2 M glycerol. Similar results are shown in Supplementary Fig. 1. The sample was excited at 280 nm and the emission spectra from 300 nm to 450 nm were recorded as described in Methods.
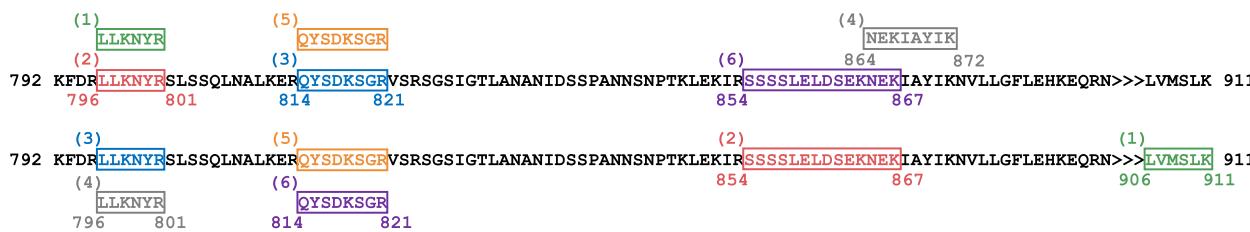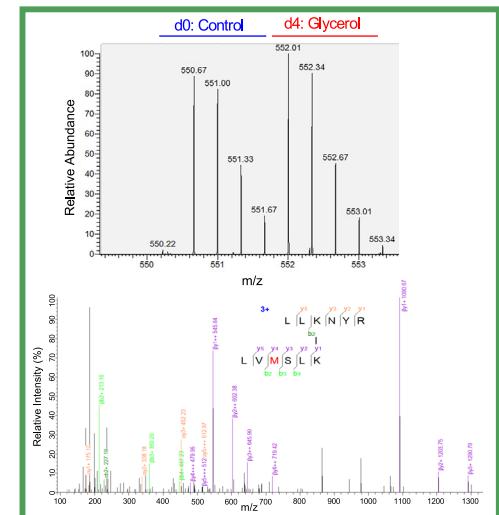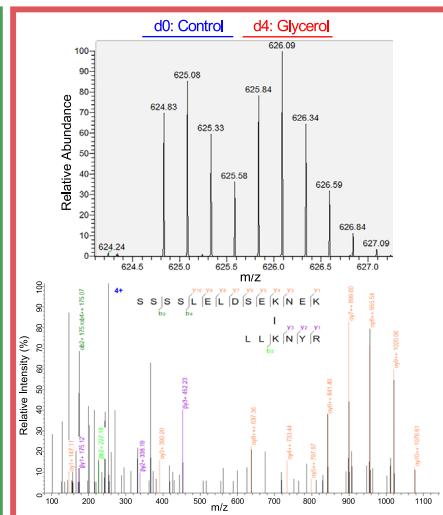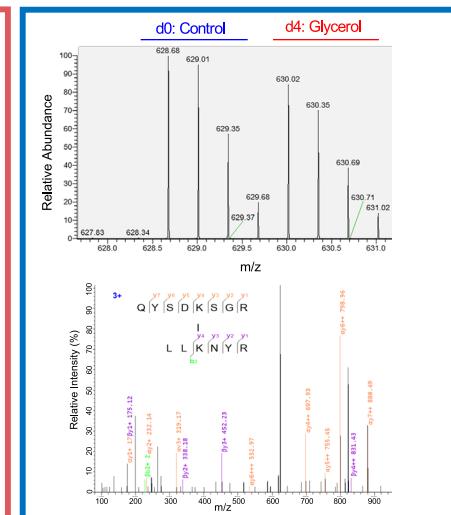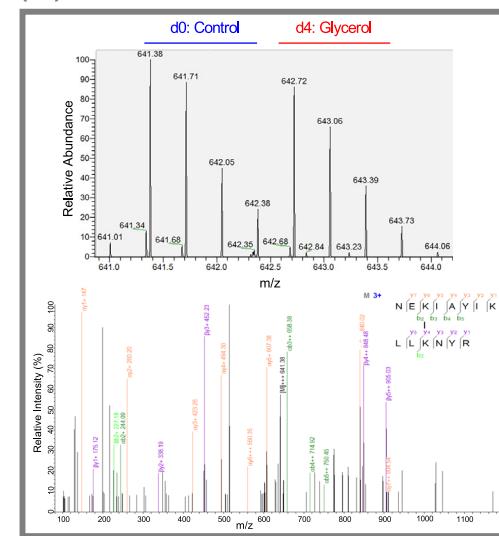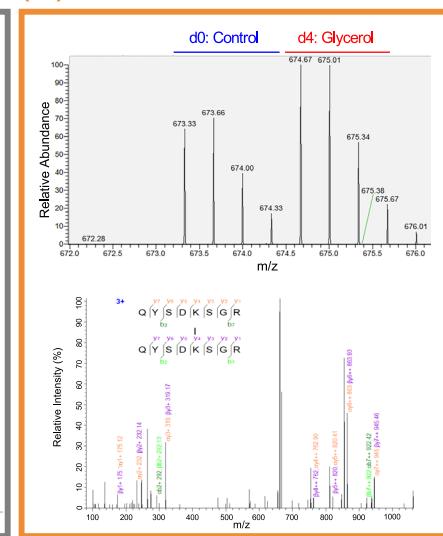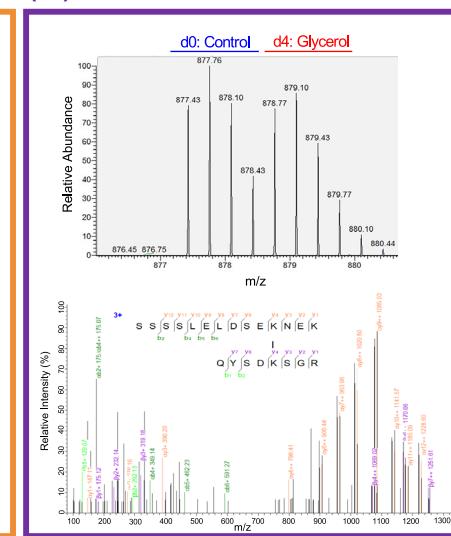
Extended Data Fig. 8 | Differential cross-linked peptide pairs on Imh1-C213 identified in the absence and presence of 0.1 M glycerol. (**a**) Six differently cross-linked peptide pairs on Imh1-C213 were identified, as highlighted in bold in Supplementary Table 1, both in the absence and presence of 0.1 M glycerol. The identified cross-linked peptide pairs are highlighted in squares, with the residues numbered according to their positions in full-length Imh1. The color and number of each square correspond to the specific cross-linked peptide pairs associated

with the six sets of spectra presented in panel **b**. (**b**) Mass spectra (MS1) and tandem mass spectra (MS2) of the six differential cross-linked peptide pairs on Imh1-C213, regulated by glycerol, are presented. The upper panel displays extracted ion chromatograms generated using Xcalibur 2.2 software (Thermo Fisher Scientific). The matches for b and y ions of the cross-linked peptides, shown in the lower panel, were annotated using pLink3 and visualized with pLabel software (version 2.4.3), as detailed in the Methods section.
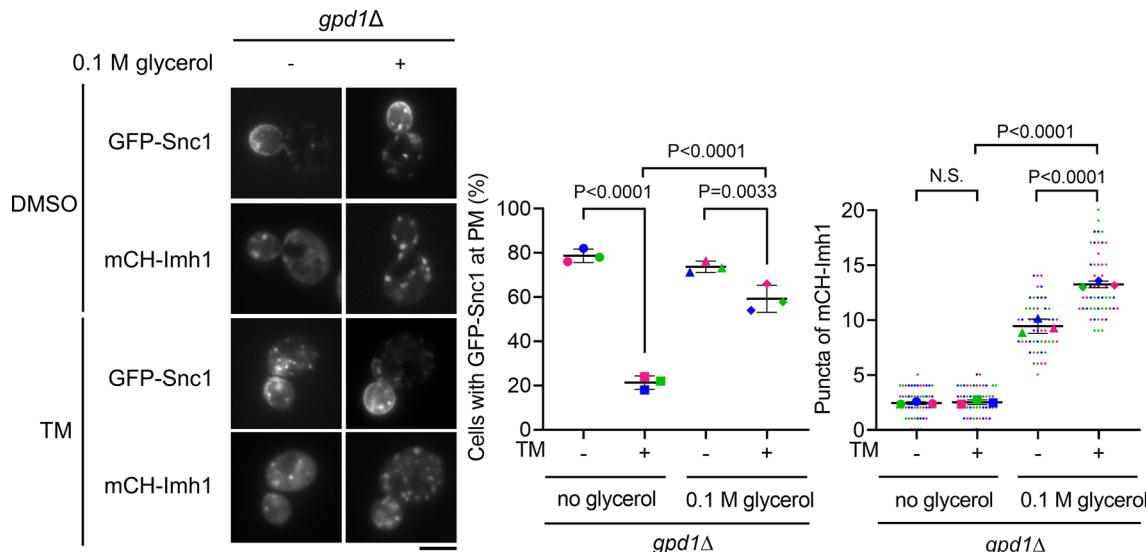
Extended Data Fig. 9 | Glycerol rescues Imh1 and Snc1 localization in *gpd1Δ* cells under ER stress. Cells expressing mCH-Imh1 and GFP-Snc1 were cultured to mid-log phase in YPD medium, and then incubated with or without 0.1 M glycerol, followed by treatment with or without 1 µg/ml TM for 1.5 h. Cells showing GFP-Snc1 plasma membrane signal were quantified (N = 3, n = 50). The number of mCH-Imh1 puncta was determined using ImageJ Fiji software (N = 3, n = 50). Data are presented as mean ± SD of three independent experiments. (N.S. Not significant; one-way ANOVA with Dunnett's post hoc multiple comparison test, no glycerol addition was used as reference). Scale bar, 5 µm.
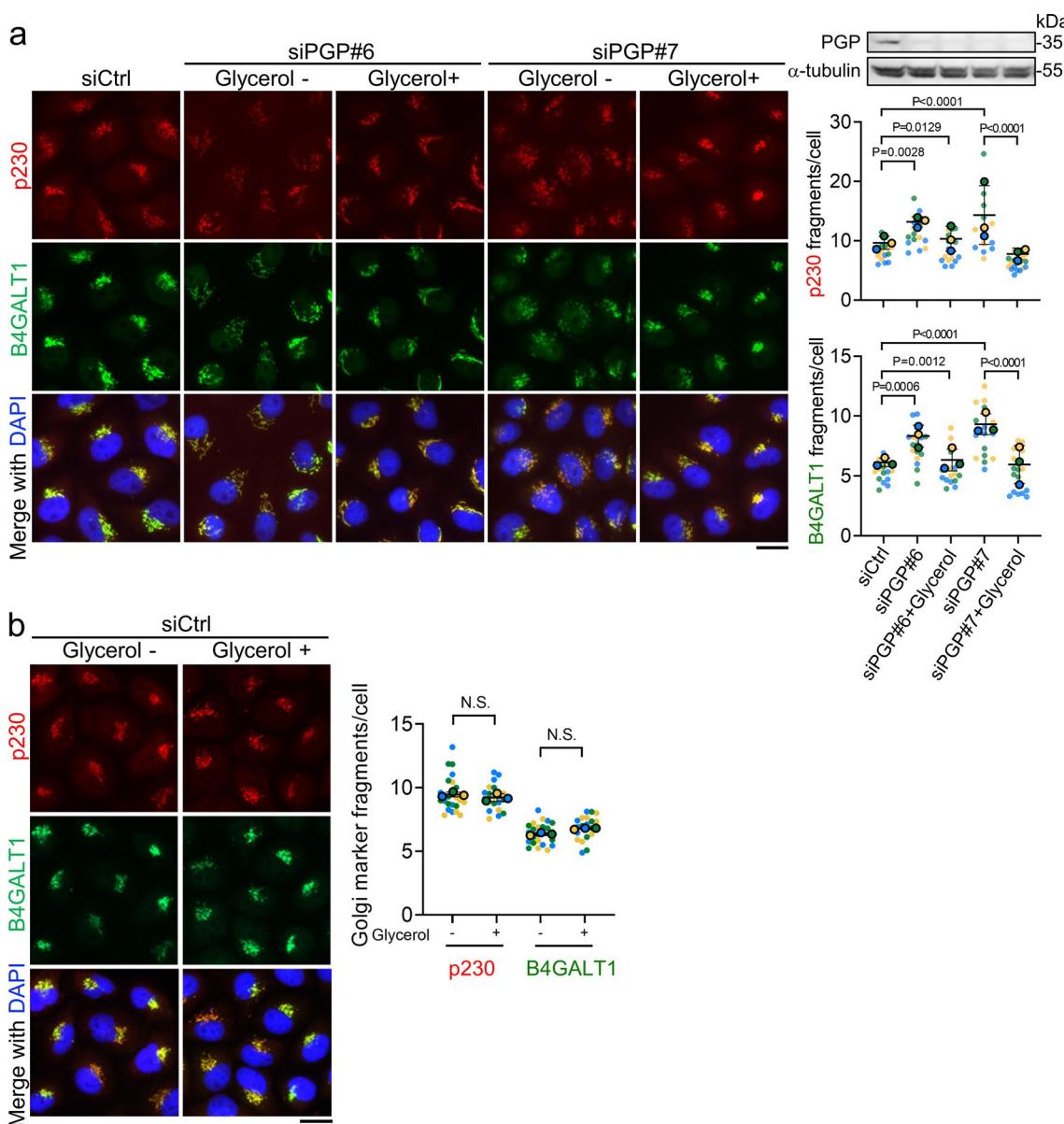
Extended Data Fig. 10 | PGP depletion-induced Golgi fragmentation can be restored by glycerol in mammalian cells. (**a**) Human PGP was knocked down by two individual siRNAs (siPGP#6 and siPGP#7) in HeLa cells to observe the subcellular localization of p230 (red) and B4GALT1 (green). Glycerol (0.1 M) was applied to the indicated groups for an additional 1 h. DAPI is the nuclear stain. Scale bar, 20 mm. PGP-knockdown efficiency was detected by western blotting. Golgi fragmentation (p230 and B4GALT1) was quantified (N = 3, n = 15). Data are reported as the mean ± SD of three independent experiments. (One-way ANOVA with Dunnett's post-hoc multiple comparison test) (**b**) HeLa cells were treated with control siRNA (siCtrl) and supplied with 0.1 M glycerol for 1 h. Subcellular localization of p230 (red), B4GALT1 (green), and DAPI (blue) were stained. Scale bar, 20 mm. Golgi fragmentation (p230 and B4GALT1) was quantified (N = 3, n = 20). Data are reported as the mean ± SD of three independent experiments. (N.S. not significant; two-sided unpaired t test). (**a-b**) Golgi fragmentation was defined by calculating the number of disconnected Golgi marker signals (shown as fragments here) detected by Imaris software. Each statistical spot represents the average vesicles/cell in an image captured at 400X magnification that containing ~35 cells. Detailed settings are described in the Methods. Data collected from the same biological replicates were labeled in the same color.

nature portfolio

Corresponding author(s): Chia-Jung Yu, Fang-Jen S. Lee

Last updated by author(s): May 10, 2025

Reporting Summary

Nature Portfolio wishes to improve the reproducibility of the work that we publish. This form provides structure for consistency and transparency in reporting. For further information on Nature Portfolio policies, see our Editorial Policies and the Editorial Policy Checklist.

Statistics

For all statistical analyses, confirm that the following items are present in the figure legend, table legend, main text, or Methods section.

n/a	Confirmed	
☐	☒	The exact sample size (*n*) for each experimental group/condition, given as a discrete number and unit of measurement
☐	☒	A statement on whether measurements were taken from distinct samples or whether the same sample was measured repeatedly
☐	☒	The statistical test(s) used AND whether they are one- or two-sided *Only common tests should be described solely by name; describe more complex techniques in the Methods section.*
☒	☐	A description of all covariates tested
☒	☐	A description of any assumptions or corrections, such as tests of normality and adjustment for multiple comparisons
☐	☒	A full description of the statistical parameters including central tendency (e.g. means) or other basic estimates (e.g. regression coefficient) AND variation (e.g. standard deviation) or associated estimates of uncertainty (e.g. confidence intervals)
☐	☒	For null hypothesis testing, the test statistic (e.g. *F*, *t*, *r*) with confidence intervals, effect sizes, degrees of freedom and *P* value noted *Give P values as exact values whenever suitable.*
☒	☐	For Bayesian analysis, information on the choice of priors and Markov chain Monte Carlo settings
☒	☐	For hierarchical and complex designs, identification of the appropriate level for tests and full reporting of outcomes
☐	☒	Estimates of effect sizes (e.g. Cohen's *d*, Pearson's *r*), indicating how they were calculated

Our web collection on statistics for biologists contains articles on many of the points above.

Software and code

Policy information about availability of computer code

Data collection	Microscopy data were collected by using a Zeiss Axioplan microscope equipped with a Cool Snap FX-camera (Carl Zeiss).The gel filtration data was collected using a HiLoad 16/600 Superdex 200 pg column (Cytiva) with an AKTA pure system (Cytiva). Data in sedimentation velocity analysis was collected by XL-A analytical ultracentrifuge equipped with UV-VIS absorbance detection system (Beckman-Coulter). The SEC–MALS measurements were performed using a miniDAWN TREOS detector (Wyatt) coupled to an Agilent 1260 Infinity HPLC. The mass photometry data was collected by TwoMP mass photometer (Refeyn). The cross-linking mass data were collected by LTQ-Orbitrap Elite Hybrid MS spectrometer (Thermo Fisher Scientific) operated with Xcalibur 2.2 software (Thermo Fisher Scientific). Intrinsic tryptophan fluorescence data was collected using an Infinite M1000 PRO microplate reader (Tecan).
Data analysis	Image data, western blot data and coomassie brilliant blue staining result was quantified by using Image J (version 1.51j8) or Imaris (version 9.8) and analyzed by GraphPad Prism 9. The gel filtration data was analyzed by UNICORN 7.3 software. Data in sedimentation velocity analysis was analyzed by SEDFIT (The parameter was calculated by SEDNTERP). SEC-MALS data was analyzed by ASTRA 6 software. The mass photometry data was analyzed by Refeyn DiscoverMP software. The raw spectral of mass spectrometry data were uploaded to the pLink3 search engine (version 3.0.16, released on 2025-01-11) to identify and quantify the cross-links. The cross-linked peptides were visualized by pLabel software (version 2.4.3).Intrinsic tryptophan fluorescence data was processed using Excel. Protein structure of His-Imh1-C213 dimer was predicted by AlphaFold3.

For manuscripts utilizing custom algorithms or software that are central to the research but not yet described in published literature, software must be made available to editors and reviewers. We strongly encourage code deposition in a community repository (e.g. GitHub). See the Nature Portfolio guidelines for submitting code & software for further information.

Data

Policy information about [availability of data](#)

All manuscripts must include a [data availability statement](#). This statement should provide the following information, where applicable:

- Accession codes, unique identifiers, or web links for publicly available datasets
- A description of any restrictions on data availability
- For clinical datasets or third party data, please ensure that the statement adheres to our [policy](#)

> The mass spectrometry data have been deposited to the ProteomeXchange Consortium via the PRIDE partner repository with the data set identifier PXD061125. The FASTA file of the Imh1-C213 sequence is derived from UniProt, with accession code Q06704. All data generated or analyzed during this study are included in this published article and its supplementary information files. Source data are provided with this paper.

Research involving human participants, their data, or biological material

Policy information about studies with [human participants or human data](#). See also policy information about [sex, gender (identity/presentation), and sexual orientation](#) and [race, ethnicity and racism](#).

Reporting on sex and gender	No human research participants
Reporting on race, ethnicity, or other socially relevant groupings	No human research participants
Population characteristics	No human research participants
Recruitment	No human research participants
Ethics oversight	No human research participants

Note that full information on the approval of the study protocol must also be provided in the manuscript.

Field-specific reporting

Please select the one below that is the best fit for your research. If you are not sure, read the appropriate sections before making your selection.

☒ Life sciences   ☐ Behavioural & social sciences   ☐ Ecological, evolutionary & environmental sciences

For a reference copy of the document with all sections, see [nature.com/documents/nr-reporting-summary-flat.pdf](#)

Life sciences study design

All studies must disclose on these points even when the disclosure is negative.

Sample size	For panels with quantification, all statistical data are displayed as the mean±SD with three biological replicates. No sample-size calculations were performed. The quantification data was acquired by one-way ANOVA with Dunnett's post hoc multiple comparison test. We determined the sample sizes by referencing our previous experiments to ensure they are sufficient for detecting significant biological differences reliably and with good reproducibility (Hsu et al., 2016, Chen et al., 2010).
Data exclusions	No data were excluded.
Replication	All experiments were performed at least three times unless otherwise indicated and the figures show representative results. The results of experiment were repeated three independently with similar results, and one representative result from each group was shown in Fig. 1, 2b-d, 3b-d, 4, 5c-d, 7, 8 a-b, and Extended Data Figure 1, 2b-d, 3b, 4, 5, 6a, 7b, 9, and 10 a,c. The mass spectrometry analysis was performed using a triplicate label-swap approach.
Randomization	No human data were used in the study. Randomization is not generally used in this field. Randomization for different experimental groups was not relevant as they were performed on uniform biological material, ie. Cell lines procured from commercial source. Due to the high reproducibility and consistency between cell cultures, it was predetermined that three biological replicates would allow for adequate analysis to reach meaniful conclusions of the data.
Blinding	Blinding is not relevant to our study because it is not clinical trial or research with different groups/participants.

Reporting for specific materials, systems and methods

We require information from authors about some types of materials, experimental systems and methods used in many studies. Here, indicate whether each material, system or method listed is relevant to your study. If you are not sure if a list item applies to your research, read the appropriate section before selecting a response.

Materials & experimental systems

n/a	Involved in the study
☐	☒ Antibodies
☐	☒ Eukaryotic cell lines
☒	☐ Palaeontology and archaeology
☒	☐ Animals and other organisms
☒	☐ Clinical data
☒	☐ Dual use research of concern
☒	☐ Plants

Methods

n/a	Involved in the study
☒	☐ ChIP-seq
☒	☐ Flow cytometry
☒	☐ MRI-based neuroimaging

Antibodies

Antibodies used	The antibodies used in this study were as follows: For western blot, the secondary antibodies used were goat horseradish peroxidase (HRP)-conjugated anti-rabbit/mouse IgG (AP132P/AP124P, Millipore, 1:5000), anti-HA (# MMS-101R, Biolegend,1:3000), anti-Myc (#2276S,1:3000),anti-PGP (A305-669A-M, BETHYL, 1:3000)and anti-α-tubulin (t5168,Sigma-Aldrich,1;5000). Anti-Imh1(1:3000), anti-Pgk1 (1:3000), and anti-Arf1 (1:3000) rabbit antibodies were generated by our laboratory as previously described (Wang et al., 2022; Lai et al., 2023). For immunofluorescence staining in mammalian cells, primary antibodies anti-B4GALT1 (ab121326, Abcam, 1:200) and anti-p230 (611281, BD, 1:100), and secondary antibodies Alexa Fluor 488/594 goat anti-rabbit and mouse IgG (A-11034/A-11012 and A-11001/A-11032, Invitrogen, 1:1000) were used.
Validation	anti-Imh1, anti-Pgk1, and anti-Arf1 rabbit antibodies-validated by ourselves as previously described (Wang et al., 2022; Lai et al., 2023). The validation statements for each commercial antibody can be found on the manufacturers' websites. anti-HA (# MMS-101R)- Suitable for: WB, ICC, IP, Flow. Reacts with: species-independent https://www.biolegend.com/fr-ch/products/anti-ha-11-epitope-tag-antibody-11071 anti-Myc (#2276S)- Suitable for: WB, IHC, IP, IF, Flow, ChIP. Reacts with: species-independent https://www.cellsignal.com/products/primary-antibodies/myc-tag-9b11-mouse-mab/2276?srsltid=AfmBOooXf63KSwwRULNL7GBNtx5IDb4DRX2T3G4V7z9z-plTbOLfJyEs anti-α-tubulin (t5168) - Suitable for: WB, IF. Reacts with: mouse, chicken, Chlamydomonas, African green monkey, human, rat, bovine, sea urchin, kangaroo rat https://www.sigmaaldrich.com/TW/zh/product/sigma/t5168?srsltid=AfmBOopX9NDdf8CuYDbYxEUmyg7ZyzrOx293vZ9ISonX4dCweZDu5Bqn anti-PGP (A305-669A-M)-Suitable for WB, IP. Reacts with: Human, Mouse https://www.thermofisher.com/antibody/product/PGP-Antibody-Polyclonal/A305-669A-T anti-B4GALT1 (ab121326)-Suitable for IHC-P, ICC, WB. Reacts with Human samples. https://www.abcam.com/en-us/products/primary-antibodies/b4galt1-antibody-ab121326?srsltid=AfmBOopxzAJufcIJRwkaE8LEomVzd0XxRlSIezELoSGqotWGB0TKsIwe anti-p230 (611281)-Suitable for WB, IF. Reacts with: Human. https://www.bdbiosciences.com/en-ca/products/reagents/microscopy-imaging-reagents/immunofluorescence-reagents/purified-mouse-anti-human-p230-trans-golgi.611281?tab=product_details Alexa Fluor 488/594 goat anti-rabbit IgG (A-11034/A-11012) -Suitable for ICC/IF, Flow. Reacts with: rabbit. https://www.thermofisher.com/antibody/product/Goat-anti-Rabbit-IgG-H-L-Highly-Cross-Adsorbed-Secondary-Antibody-Polyclonal/A-11034 https://www.thermofisher.com/antibody/product/Goat-anti-Rabbit-IgG-H-L-Cross-Adsorbed-Secondary-Antibody-Polyclonal/A-11012 Alexa Fluor 488/594 goat anti-mouse IgG (A-11001/A-11032)-Suitable for IHC, ICC/IF, Flow. Reacts with: mouse. https://www.thermofisher.com/antibody/product/Goat-anti-Mouse-IgG-H-L-Cross-Adsorbed-Secondary-Antibody-Polyclonal/A-11001 https://www.thermofisher.com/antibody/product/Goat-anti-Mouse-IgG-H-L-Highly-Cross-Adsorbed-Secondary-Antibody-Polyclonal/A-11032 goat horseradish peroxidase (HRP)-conjugated anti-rabbit IgG (AP132P)-Suitable for ELISA, IHC, WB. Reacts with: Specific for rabbit IgG, heavy and light chain. https://www.merckmillipore.com/TW/zh/product/Goat-Anti-Rabbit-IgG-Antibody-Peroxidase-Conjugated,MM_NF-AP132P?ReferrerURL=https%3A%2F%2Fwww.google.com%2F goat horseradish peroxidase (HRP)-conjugated anti-rmouse IgG (AP124P)-Suitable for ELISA, IHC, WB. Reacts with: mouse IgG under native and reduced conditons. Under reduced conditions cross reactivity to non-mouse IgG may be seen because of similarity of immunoglobulin chains. https://www.merckmillipore.com/TW/zh/product/Goat-Anti-Mouse-IgG-Antibody-Peroxidase-Conjugated-HL,MM_NF-AP124P?

Eukaryotic cell lines

Policy information about cell lines and Sex and Gender in Research

Cell line source(s)	Human epithelial cell line HeLa (CCL-2) is from ATCC.
Authentication	Cell line was authenticated using short tandem repeat analysis.
Mycoplasma contamination	Fluorescent DNA staining using Hoechst 33258 confirmed cell cultures to be mycoplasma-free.
Commonly misidentified lines (See ICLAC register)	No commonly misidentified cell line was used in the study.